

# Low- $z$ Mg II Broad Absorption-Line Quasars from the Sloan Digital Sky Survey

Shaohua Zhang<sup>1,2</sup>, Ting-Gui Wang<sup>1,2</sup>, Huiyuan Wang<sup>1,2</sup>, Hongyan Zhou<sup>1,2</sup>, Xiao-Bo Dong<sup>1,2</sup>,  
Jian-Guo Wang<sup>3,4,5</sup>

## ABSTRACT

We present a sample of 68 low- $z$  Mg II low-ionization broad absorption-line (loBAL) quasars. The sample is uniformly selected from the Sloan Digital Sky Survey Data Release 5 according to the following criteria: (1) redshift  $0.4 < z \leq 0.8$ , (2) median spectral  $S/N > 7 \text{ pixel}^{-1}$ , and (3) Mg II absorption-line width  $\Delta v_c \geq 1600 \text{ km s}^{-1}$ . The last criterion is a trade-off between the completeness and consistency with respect to the canonical definition of BAL quasars that have the ‘balnicity index’  $BI > 0$  in C IV BAL. We adopted such a criterion to ensure that  $\sim 90\%$  of our sample are classical BAL quasars and the completeness is  $\sim 80\%$ , based on extensive tests using high- $z$  quasar samples with measurements of both C IV and Mg II BALs. We found (1) Mg II BAL is more frequently detected in quasars with narrower  $H\beta$  emission-line, weaker [O III] emission-line, stronger optical Fe II multiplets and higher luminosity. In term of fundamental physical parameters of a black hole accretion system, loBAL fraction is significantly higher in quasars with a higher Eddington ratio than those with a lower Eddington ratio. The fraction is not dependent on the black hole mass in the range concerned. The overall fraction distribution is broad, suggesting a large range of covering factor of the absorption material. (2) [O III]-weak loBAL quasars averagely show undetected [Ne V] emission line and a very small line ratio of [Ne V] to [O III]. However, the line ratio in non-BAL quasars, which is much larger than that in [O III]-weak loBAL quasars, is independent of the strength of the [O III] line. (3) loBAL and non-loBAL quasars have similar colors in near-infrared to optical band but different colors in ultraviolet. (4) Quasars with Mg II absorption lines of intermediate width are indistinguishable from the non-loBAL quasars in optical emission line properties but their colors are similar to loBAL quasars, redder than non-BAL quasars. We also discuss the implication of these results.

---

<sup>1</sup>Key Laboratory for Research in Galaxies and Cosmology, The University of Sciences and Technology of China, Chinese Academy of Sciences, Hefei, Anhui 230026, China; zsh, whywang@mail.ustc.edu.cn, twang@ustc.edu.cn

<sup>2</sup>Department of Astronomy, University of Science and Technology of China, Hefei, Anhui 230026, China

<sup>3</sup>National Astronomical Observatories/Yunnan Observatory, Chinese Academy of Sciences, P.O. Box 110, Kunming, Yunnan 650011, China

<sup>4</sup>Graduate School of the Chinese Academy of Sciences, 19A Yuquan Road, P.O. Box 3908, Beijing 100039, China

<sup>5</sup>Laboratory for the Structure and Evolution of Celestial Bodies, Chinese Academy of Sciences, PO Box 110, 650011 Kunming, China

*Subject headings:* galaxies: active — quasars: absorption lines — quasars: emission lines — quasars: general

## 1. Introduction

About 15% of quasars show broad absorption lines (BALs) of high ionization ions such as N V, C IV, Si IV, Ly $\alpha$ , O VI, up to a velocity of  $v \sim 0.1 c$ . BALs are detected occasionally (another  $\sim 15\%$ ) also in low ionization species such as Mg II, Al III. Two very different scenarios have been proposed to explain the BAL phenomenon. The first scenario, namely ‘unification model’, suggests that BAL and non-BAL quasars are physically the same, and attributes their different appearance solely to different line of sight. According to the unification model, every quasar has a BAL region (BALR) with a covering factor of 10%-20%, and our line of sight passes through BALR only in BAL quasars, plausibly at low inclination angles (Tolea et al. 2002; Hewett & Foltz 2003; Reichard et al. 2003b; Trump et al. 2006; Gibson et al. 2009, hereafter G09). The second, so called evolutionary scenario, suggests that BAL quasars are in the early stage of quasar evolution with a gas/dust richer nuclear environment (Sanders et al. 1988; Hamann & Ferland 1993; Voit et al. 1993; Egami et al. 1996; Becker et al. 2000; Trump et al. 2006).

On the one hand, there are many pieces of observational evidence for the unification of BAL and non-BAL quasars, including the similarity of emission line spectrum between the two classes of quasars (Weymann et al. 1991), a small covering factor of BALR inferred from emission line profiles (Korista et al. 1993), spectropolarimetric observations of BAL quasars (e.g., Goodrich & Miller 1995; Cohen et al. 1995; Hines & Wills 1995; Ogle et al. 1999; Schmidt & Hines 1999), and the great similarity of the spectral energy distribution (SED) between BAL and non-BAL quasars in the infrared to millimeter waveband (e.g., Willott et al. 2003; Gallagher et al. 2007). The notoriously weak X-ray emission from BAL quasars is often ascribed to strong absorption in the BAL direction, which is also supported by X-ray spectroscopy (e.g., Green et al. 1995; Brinkmann et al. 1999; Wang et al. 1999; Brandt et al. 2000; Gallagher et al. 2002, 2006; Fan et al. 2009). On the other hand, there are observations that cannot be understood in the simple unification scenario. First, radio morphology and radio variability study showed that BAL quasars are not observed at any preferred direction with respect to the radio axis (Jiang & Wang 2003; Brotherton et al. 2006; Zhou et al. 2006b; Ghosh & Punshly 2007; Wang et al. 2008a). Second, Boroson (2002) found that BAL quasars on average have higher Eddington ratios than non-BAL quasars in a small sample of BAL QSOs. A similar conclusion has been reached by Ganguly et al. (2007). It has also been suggested that BAL quasars are redder and more luminous than other quasars (Reichard et al. 2003b, Trump et al. 2006, cf., G09). The latter results indicate that BAL and non-BAL quasars can be unified, but the covering factor of BALR depends on their nuclear parameters. A wide range of covering factor of BALR has also been implied by comparison of the optical polarization between BAL and non-BAL quasars (Wang et al. 2005).

Significant differences between low-ionization BAL (loBAL) and high-ionization BAL (HiBAL)/non-

BAL quasars are also seen in dust extinction and far-infrared emission. loBAL quasars show a redder spectrum than HiBAL and non-BAL quasars on average, consistent with a reddening of  $E(B - V) \sim 0.1$  for a SMC-like dust extinction curve (Weymann et al. 1991; Richards et al. 2003). Dai et al. (2008) showed that BAL fraction among Two Micron All Sky Survey(2MASS) selected quasars are as high as  $\sim 44\%$  (cf. Ganguly & Brotherton 2008). Surprisingly, when going down to a low flux limit in near infrared, Maddox & Hewett (2008) found a similar 30% fraction of BAL quasars. This indicates that BAL quasars on average are heavily reddened and thus many red BAL quasars have been overlooked in optical spectroscopic surveys. This can be interpreted physically in two very different scenarios: either BAL quasars are a distinct population with the nuclei preferring a gas and dust rich environment; or dust is preferably distributed in the outflow direction as suggested by the dusty disk wind models for BALR (Konigl & Kartje 1994), and overall covering factor is 30%. Isotropic properties, such as far-infrared emission, are of great importance to distinguish between the two. Boroson & Meyers (1992) found that the fraction of loBAL quasars in a small far infrared selected sample is much higher than that in optically selected samples. They also found that these quasars show weak [O III] and strong optical Fe II emission lines. A large sample of low- $z$  loBAL quasars are needed to confirm these findings.

Low- $z$  BAL quasars are of great interest also because a number of important spectral diagnostics can be accessed via the ground optical spectroscopic observations, such as narrow emission-lines (NELs), Balmer and Fe II broad emission lines (BELs). We can also inspect the properties of the host galaxies much easier at low- $z$ . However, previous studies mainly focused on high- $z$  BAL or HiBAL quasars due to the rarity of loBAL quasars. With the advent of large area spectroscopic surveys, such as the Sloan Digital Sky Survey (SDSS; York et al. 2000), it is possible to perform a systematic study of low- $z$  BAL quasars based on a large sample.

In this paper, we present a sample of 68 Mg II BAL quasars at  $0.4 < z \leq 0.8$  uniformly selected from the quasar sample of SDSS Data Release 5 (Schneider et al. 2007), and make a comparison study with non-BAL quasars. This paper is organized as follows. We analyze the SDSS spectra and compile the sample in §2. Various definition criteria have been adopted in previous studies, and different criteria result in different fractions of BAL quasars. We have made extensive tests for different criteria in order to obtain a more objective definition of loBAL quasars. The tests are described in detail in this section, together with the definition criterion that is used in our sample. In §3, we compare the properties between loBAL and non-BAL quasars. The implication of our findings is discussed in §4. Throughout this paper, we assume a  $\Lambda$ -dominated cosmology with  $H_0 = 72 \text{ km s}^{-1} \text{ Mpc}^{-1}$ ,  $\Omega_M = 0.28$ , and  $\Omega_\Lambda = 0.72$ .

## 2. Sample Compilation and Data Analysis

We start from the SDSS DR5 quasar catalog (Schneider et al. 2007), and select 34037 quasars with redshifts of  $0.4 < z < 1.97$  and a median signal-to-noise ratio of  $S/N > 7 \text{ pixel}^{-1}$  as the parent sample of Mg II BAL quasars. The  $S/N$  ratio threshold is introduced to ensure reliable

measurements of continua and absorption and emission lines. The redshift cutoffs are so chosen that Mg II falls in the wavelength coverage of the SDSS spectrograph ( $\sim 3800 - 9200 \text{ \AA}$ ). We split the parent sample into ‘low- $z$  ( $N = 7229$ )’, ‘moderate ( $N = 16621$ )’ and ‘high- $z$  ( $N = 10187$ )’ samples with  $0.4 < z \leq 0.8$ ,  $0.8 < z \leq 1.53$ , and  $1.53 < z < 1.97$ , respectively. We will focus on the low- $z$  sample and cull our low- $z$  Mg II BAL quasars according to an objective criterion obtained from extensive tests using the high- $z$  sample with both Mg II and C IV measured. The SDSS spectra are corrected for the Galactic extinction using the extinction map of Schlegel et al. (1998) and the reddening curve of Fitzpatrick (1999), and transformed into the rest frame using the redshifts in Schneider et al. (2007) before further analysis.

### 2.1. Fitting of Mg II Spectral Regime

We fit the spectrum of Mg II regime in the following three steps.

- (1) **Determination of continuum and UV Fe II multiplets.** We fit the SDSS spectra in the rest-frame wavelength range of  $2100 - 3100 \text{ \AA}$  with a combination of a single power-law and an Fe II template. The initial values of the normalization and power-law slope are estimated from continuum windows ( $[1790, 1830] \text{ \AA}$ ,  $[2225, 2250] \text{ \AA}$  and  $[4020, 4050] \text{ \AA}$ ) that are not seriously contaminated by emission-lines (e.g., Forster et al. 2001). We adopt the Fe II template derived by Vestergaard & Wilkes (2001) and convolve it with a Gaussian kernel in velocity space to match the width of Fe II multiplets in the observed spectra. Prominent emission-lines other than Fe II are masked during the fit.
- (2) **Modeling Mg II emission line.** After subtracting the modeled power-law continuum and Fe II multiplets, we fit the residual spectrum around Mg II with one or two Gaussians. We find that two Gaussians are sufficient to reproduce Mg II line profile in most cases, and adding more component does not significantly improve the fit. The weights of Mg II blue wing are reduced to half of that of the red wing in order to lessen the effect of potential Mg II absorption troughs.
- (3) **Remodeling of the spectra.** We mask the spectral regions where the observed data are lower than 90% of the sum of the continuum and emission line models, and refit the spectra. The deficit may result from absorption-lines.

We do not include other UV emission lines, such as Fe III, [Ne IV], and [C II], which do not fall in the SDSS wavelength coverage for many quasars in the low- $z$  sample. This does not affect the measurement of Mg II absorption line. The fit is performed by minimizing  $\chi^2$ . The final model consists of a single power law for the continuum, the empirical template for UV Fe II multiplets, and one or two Gaussian for Mg II emission line. It is worthy noting that our final model does not include intrinsic dust extinction. We have tried to fit spectra with reddening as a free parameter, and found that the reddening and spectral continuum slope are degenerate. A similar result has

been found in Reichard et al. (2003a). As can be seen in Fig. 1 (see also Fig. 3), this simple model can reproduce the observed data very well for most quasars. We normalize the observed spectra using the best-fit models, and measure Mg II absorption line, if present, in the normalized spectra. We will validate in §2.3 the reliability of our Mg II absorption line measurements by a careful comparison with previous independent measurements that appeared in the literature.

## 2.2. Criteria for Mg II BAL Quasars

Both of absorption-line width and depth vary from object to object, and their distribution is broad and smooth. Upon that the fraction of BAL quasars depends strongly on the definition. Mg II is more subtle than C IV because (1) loBALs are usually narrower than HiBALs and (2) Mg II is actually a doublet with a velocity offset of  $768 \text{ km s}^{-1}$ . In this subsection, we will compare different definitions that have appeared in the literature and obtain a more objective criterion of Mg II BAL.

Weymann et al. (1991) proposed the first quantitative definition of BAL by introducing the ‘balnicity index’ (or  $BI$  for short) to describe BAL strength, which is defined as

$$BI = \int_{v_l=3,000}^{v_u=25,000} \left[1 - \frac{f(-v)}{0.9}\right] C dv, \quad (1)$$

where  $f(-v)$  is the normalized spectrum, and the velocity  $v$  in units of  $\text{km s}^{-1}$  with respect to the quasar emission-lines (negative value indicates blueshift). The weight  $C$  is set to 1 when the observed spectrum falls at least 10% below the model of continuum plus emission lines in a contiguous velocity interval ( $\Delta v_c$ ) of at least  $2000 \text{ km s}^{-1}$ , and  $C = 0$ , otherwise. The conservative value of 10% is chosen to ensure that the deficit is not caused by the uncertainty in the model of continuum and emission lines. BAL quasars are defined as objects with  $BI > 0$  in at least one absorption line.

Mg II BAL troughs are generally weaker and narrower than those found in C IV, and they usually show smaller blueshift than C IV (Voit et al. 1993; Trump et al. 2006; G09). Some bona fide BAL quasars would be lost if the same ‘ $BI$ ’ definition is adopted for Mg II. With this consideration in mind, a few authors suggested to modify  $BIs$  by changing the starting velocity and/or the interval of contiguous absorption in the Eq.1. Hall et al. (2002) redefined the starting velocity  $v_l = 0 \text{ km s}^{-1}$  and a minimum contiguous interval of  $450 \text{ km s}^{-1}$  to give the ‘absorption index’ ( $AI$  for short), and selected loBAL quasars according to the criterion of  $AI > 0 \text{ km s}^{-1}$ . Trump et al. (2006) modified this definition slightly so that  $AI$  is a true equivalent width, measuring all absorption within the limits of every absorption trough. Their  $AI$  is defined as

$$AI = \int_{v_l=0}^{v_u=29,000} [1 - f(-v)] C' dv, \quad (2)$$

where  $C' = 1$  when  $\Delta v_c > 1000 \text{ km s}^{-1}$  at a depth of  $>10\%$  continuum; otherwise,  $C' = 0$ .

Tolea et al. (2002) found that  $BI$  distribution is very broad, and there is no bimodality for BAL quasars in the SDSS early data release. They pointed out that the definition is subjected to certain arbitrariness (see also Weymann 2002). However, Knigge et al. (2008) claimed that logarithmic  $AI$  shows a bimodal distribution and argued that  $BI$  works fairly well. Similarly, G09 introduced a modified  $BI$ , namely  $BI_0$  by expanding the integral from  $v_l=0 \text{ km s}^{-1}$ , and they calculated both  $BI$  and  $BI_0$  for each ion (Si IV, C IV, Al III, and Mg II). We set a maximum integration velocity of Mg II BALs to  $20,000 \text{ km s}^{-1}$  to avoid confusion of Fe II resonant absorption lines because Mg II BALs rarely extend to such a large velocity. So, in this work the upper and lower limits on velocity for  $AI$  integral are  $20,000 \text{ km s}^{-1}$  and  $0 \text{ km s}^{-1}$ . The definitions for BAL quasar are summarized in Table 1.

Since all known loBAL quasars show HiBALs, we can check consistency of different definition of loBAL with that of HiBAL quasars based on the presence of C IV BAL. With both Mg II and C IV measurable, the high- $z$  quasar sample is well suited for this purpose. We compare the fraction of C IV HiBAL, which is defined as  $BI_0 > 0$  (G09) among the loBAL quasar candidates with various  $\Delta v_c$  cutoff in Mg II  $AI$  definition. We search for Mg II BAL using different  $\Delta v_c$ , from 800 to  $2000 \text{ km s}^{-1}$  with an interval of  $\delta v = 200 \text{ km s}^{-1}$ . The numbers of Mg II BAL quasar candidates are 395, 152, 119, 93, 73, 49 and 40, for  $\Delta v_c \geq 800, 1000, 1200, 1400, 1600, 1800$  and  $2000 \text{ km s}^{-1}$ , respectively. We cross-match these candidates with the HiBAL quasar catalog of G09, and find that the fraction of HiBAL quasars in each bin between two successive widths,  $p(\Delta v_i, \Delta v_i + \delta v)$ , increases with increasing  $\Delta v_i$ . Specifically, all but three loBAL quasar candidates with  $\Delta v_c \geq 1800 \text{ km s}^{-1}$  show C IV BALs, and about 79% of the candidates do for  $1600 \leq \Delta v_c < 1800 \text{ km s}^{-1}$ . The percentage drops quickly as the velocity cutoff decreases, for example  $p(1200, 1400) \sim 42\%$  and  $p(1000, 1200) \sim 27\%$ . For  $800 \leq \Delta v_c < 1000 \text{ km s}^{-1}$ , only  $p \sim 15\%$  of the Mg II BAL quasar candidates show C IV BAL, which is similar to the fraction of HiBAL quasars found in optically selected samples.

Assuming an average C IV BAL fraction of 15% for optically-selected quasars, we can estimate the true fraction of Mg II BAL quasars in each bin approximately as follows:

$$x(\Delta v_0 + i\delta v, \Delta v_0 + (i + 1)\delta v) = \frac{p(\Delta v_0 + i\delta v, \Delta v_0 + (i + 1)\delta v) - 0.15}{1 - 0.15}, \quad \text{for } i = 0, 1, 2, 3, \dots \quad (3)$$

where  $\Delta v_0 = 800 \text{ km s}^{-1}$ .

The ‘correctness’  $c1$  and ‘completeness’  $c2$  as a function of Mg II absorption-line width cutoff  $\Delta v_c$  can be estimated as follows,

$$c1(\Delta v_c \geq \Delta v_i) = \frac{\sum_{j=0}^{\infty} x(\Delta v_i + j\delta v, \Delta v_i + (j + 1)\delta v) \times N(\Delta v_i + j\delta v, \Delta v_i + (j + 1)\delta v)}{N(\Delta v_c \geq \Delta v_i)}, \quad (4)$$

$$c2(\Delta v_c \geq \Delta v_i) = \frac{\sum_{j=0}^{\infty} x(\Delta v_i + j\delta v, \Delta v_i + (j+1)\delta v) \times N(\Delta v_i + j\delta v, \Delta v_i + (j+1)\delta v)}{\sum_{j=0}^{\infty} x(\Delta v_0 + j\delta v, \Delta v_0 + (j+1)\delta v) \times N(\Delta v_0 + j\delta v, \Delta v_0 + (j+1)\delta v)} \quad (5)$$

where  $N$  is the number of Mg II BALs in the width bin between two neighbor width cutoffs and a reasonable criterion should be well balanced between ‘correctness’ and ‘completeness’. The cutoff  $\Delta v_i \approx 1600 \text{ km s}^{-1}$  serves as a good trade-off between the ‘correctness’ and ‘completeness’ (see Fig. 2). Using such a definition criterion, we have a correctness of  $c1(\Delta v_c \geq 1600 \text{ km s}^{-1}) \approx 87.10\%$  and a completeness of  $c2(\Delta v_c \geq 1600 \text{ km s}^{-1}) \approx 78.30\%$ . We have visually examined the Mg II absorption-line profile, and found that it very often splits into doublet for  $\Delta v_c < 1600 \text{ km s}^{-1}$ , while it generally shows a smooth profile for  $\Delta v_c \geq 1600 \text{ km s}^{-1}$ . This also suggests that  $\Delta v_c \geq 1600 \text{ km s}^{-1}$  is a natural choice for defining loBAL quasars.

### 2.3. Reliability of Mg II Absorption-Line Measurements and BAL Classifications

Adopting above criterion, we culled 68 low- $z$  Mg II BAL quasars. The observed spectra and fits are displayed in Fig. 3, and the properties of absorption and emission lines are summarized in Table 2. In this subsection, we examine the reliability of our Mg II absorption-line measurements and BAL classifications by comparing with G09.

In the low- $z$  sample, 49 quasars are classified as Mg II BAL quasars by G09 according to the criterion of  $BI_{0,Mg II} > 0$ . Forty-one of them also fulfill our new criterion (marked with “B” in Fig. 3). In Fig. 4, we compare our measurements of  $EW_{absor}$ ,  $V_{min}$  and  $V_{max}$  with those of G09. For most quasars, our measurements are the same as G09. Large discrepancies in the minimum velocity are found for three quasars (J1012+4921, J1044+3656 & J1321+0202). Those quasars show two absorption troughs, and G09 measured the larger velocity one, while we consider both troughs (Fig 3). Significant difference in  $V_{max}$  is found in three quasars J1259+1213, J2107-0620 and J1321+0202. In the former two, Mg II BALs are potentially affected by Fe II absorption lines, and our  $AI$  integral is up to 20,000  $\text{km s}^{-1}$  only, so the measured  $V_{max}$  are less than these of G09. The third one is likely caused by different continuum modeling: G09 did not include UV Fe II model, while we do.

We also find that eight Mg II BAL quasars in G09’s sample do not fulfill our new criterion. Fig. 3 shows the observed spectra and our best-fit models for these ‘lost’ Mg II BAL quasars (marked with “L”). We divide them into three cases: (1) no absorption line. We do not detect absorption troughs at the level at least 10% below the best fitted continuum and emission line model in three objects. Mg II falls near the edge of SDSS spectral coverage for two of them (J1015+3915 and 1018+5726), while the third object (J1142+0709) show strong Fe II emission lines. G09 did not include UV Fe II in their mod3el and Mg II emission line is fitted with Voigt profile; while we properly take into account UV Fe II and adopt two Gaussian for Mg II emission line. Different model should account for the difference in the BAL classification in the last case. (2) narrow absorption line. We measure only narrow absorption troughs in other four objects (J0848+0345,

J1051+5250, J1400+3539 and J1426+4112). The difference is attributed to different approach of continuum and emission line modeling. (3) J0802+5513. This object displays a redshifted Mg II BAL, relative to the systematic redshift ( $z = 0.663 \pm 0.001$ ) measured from NELs, such as [O II] and [O III], thus main part of Mg II BAL falls out the integration range of absorption line index. With  $V_{min}=19,935 \text{ km s}^{-1}$  and  $V_{max}=24,466 \text{ km s}^{-1}$ , G09 probably took the Fe II absorption trough as the Mg II BAL.

In our loBAL quasar sample, there are 27 objects which are not included in G09’s sample, we also show their spectra marked with "A" in Fig. 3. More than half of them (15) have absorption line width  $1600 \leq \Delta v_c < 2000 \text{ km s}^{-1}$ , while nearly a half sources have  $\Delta v_c \geq 2000 \text{ km s}^{-1}$  including five quasars (J0911+4035, J1133+1112, J1250+4021, J1632+4204 and J1652+2158)  $\Delta v_c \gg 2000 \text{ km s}^{-1}$ . Thus the difference between our sample and G09 is caused by the continuum and emission line modeling, as well as the different definition of Mg II BAL. Noting that most loBAL quasars with  $1600 \leq \Delta v_c < 2000 \text{ km s}^{-1}$  show smooth, broad and deep absorption troughs, just like loBAL quasars selected by  $\Delta v_c \geq 2000 \text{ km s}^{-1}$ , except for two sources, 1129+4228 and 1339+1119. Therefore most of them should be Mg II BAL quasars, and our measurements should be as reliable as G09.

## 2.4. Measurement of Emission Line and Continuum Parameters

Our low- $z$  sample of Mg II BAL quasars enable us to explore the properties of many optical emission lines. We measured in the SDSS spectra the parameters of broad and narrow optical emission lines, including  $H\gamma$ ,  $H\beta$ , Fe II, [Ne V] $\lambda$  3425, [O II] $\lambda$  3728, [Ne III] $\lambda$  3869, [O III]  $\lambda\lambda$  4959, 5007 as well as the continuum slope and normalization. The procedure of the fitting is described in detail in Dong et al. (2008), and we will only briefly outline it here. The optical continuum from 3600Å to 5300 Å is approximated by a single power-law. Fe II multiplets, both broad and narrow, are modeled using the I Zw 1 templates provided by Véron-Cetty et al. (2004). Emission lines are modeled as multiple Gaussians: at most four Gaussians for broad  $H\beta$ , one or two Gaussians for [O III]<sup>6</sup>, and one Gaussian for each of the other NELs. We assume that the [O III] doublet have the same redshift and profile, and fix their doublet ratio [O III]4959/5007 to its theoretical value. The equivalent widths of broad and narrow optical Fe II multiplets in the composite spectra are calculated as follows:  $EW_{OptFeII} = \int_{4200\text{Å}}^{5800\text{Å}} f_{OptFeII}(\lambda)/f_{con}(\lambda)d\lambda$ , where,  $f_{OptFeII}$  is the flux of broad or narrow optical Fe II emission,  $f_{con}$  is the continuum flux.

We measure the continuum slope  $\beta_{[3K,4K]}$  ( $F_\lambda \propto \lambda^{\beta_{[3K,4K]}}$ ) between  $\sim 3000 \text{ Å}$  and  $\sim 4000 \text{ Å}$  for all quasars in the low- $z$  sample. The two continuum windows, [3010, 3040]Å and [4210,

---

<sup>6</sup>The [O III] $\lambda$ 5007 profile often shows an extended blue wing and a sharp red falloff (Heckman et al 1981). We fit each of the [O III] doublets with two Gaussians when the blue wing is significant. We set upper-limits of 400  $\text{km s}^{-1}$  and 500  $\text{km s}^{-1}$  to the line shift and the  $\sigma$  of the broad Gaussian, respectively.



4332]Å, are so chosen to avoid strong Fe II multiplets shortward of 3000 Å, and possible star-light contribution longward of 5000 Å in some quasars. It is worthy to mention that these bands are still affected by the Balmer continuum, and significant Fe II emission, though small. The slope thus may not represent correctly the underlying intrinsic continuum in individual quasar. However, it can be used as an indicator of continuum reddening in a statistical way.

Using the measured continuum and emission line parameters, we estimate black hole mass  $M_{BH}$ , using empirical relation between black hole mass and the continuum luminosity and broad line width, and Eddington ratio  $L_{bol}/L_{Edd}$  for all quasars. The presence of H $\beta$  emission line is important for the black hole mass estimate because BAL associated with Mg II often introduces a large uncertainty in the measurement of Mg II line width. The black hole mass is estimated using the following prescription (Vestergaard & Peterson 2006):

$$\log M_{BH}(H\beta) = \log \left[ \left( \frac{FWHM(H\beta)}{1000 \text{ km s}^{-1}} \right)^2 \left( \frac{\lambda L_{\lambda}(5100 \text{ \AA})}{10^{44} \text{ erg s}^{-1}} \right)^{0.50} \right] + (6.91 \pm 0.02). \quad (6)$$

where, FWHM(H $\beta$ ) is the full width at half-maximum of H $\beta$ , after subtracting the narrow component. The bolometric luminosity  $L_{bol}$  is estimated from the monochromatic luminosity at 5100Å,  $\lambda L_{\lambda}(5100\text{\AA})$ , with a bolometric correction of 9 (Kaspi et al. 2000).

### 3. RESULT AND ANALYSIS

#### 3.1. Dust Extinction in Mg II BAL Quasars

It is known that that BAL quasars in general have redder continua than non-BAL quasars, and loBAL quasars are even redder than HiBAL quasars (Weymann et al. 1991; Brotherton et al. 2001; Reichard et al. 2003b; Trump et al. 2006; G09). The red color of BAL quasars is usually ascribed to the dust reddening in the BAL direction. We plot the probability distributions of  $\beta_{[3K,4K]}$  in Fig. 5 panel (a) for both of Mg II BAL quasars and non-Mg II BAL quasars. Their distributions are both skewed to the red. The skewness in the non-BAL quasars is likely due to dust reddening (Richards et al. 2003). Although the width of the distributions for BAL and non-BAL quasars are quite similar, BAL quasars are much redder than non-BAL quasars. In fact, all but two Mg II BAL quasars have  $\beta_{[3K,4K]} > -2.2$ , which is the median value for non-BAL quasars. The larger  $\beta_{[3K,4K]}$  values of Mg II BAL quasars are very likely due to excess dust reddening in loBAL quasars as will be discussed in the next section. Interestingly, seven Mg II BAL quasars have very red color of  $\beta_{[3K,4K]} > -0.2$ , which form the red peak in Fig. 5 panel (a). We visually inspected their observed spectra and found that this results from significant contribution of starlight of their host galaxies. Follow-up optical spectroscopy with a high  $S/N$  ratio will be able to reveal the properties of their host galaxies.

We further compare the broad band SED between Mg II BAL and non-Mg II BAL quasars, from ultraviolet through optical to near-infrared in quasar rest-frame. We cross-correlate our low- $z$

quasar sample against the 2MASS point source catalog (Skrutskie et al. 2006), and found 1993 matches within  $1''$  offset between the optical and near-infrared positions. Among them, 33 (or 1.7%) objects are Mg II BAL quasars. As can be seen in Fig. 6, the rest-frame near-infrared to optical colors of Mg II BAL and non-BAL quasars are essentially the same, while the former are significantly redder than the latter in the ultraviolet. This result is consistent with the interpretation of the red color of loBAL quasars as dust reddening.

### 3.2. Composite Spectra of Mg II BAL Quasars

To compare the average properties of non-Mg II BAL quasars and Mg II BAL quasars, we created a geometric mean (composite) spectrum for each class, following Vanden Berk et al. (2001). For each quasar, we measure its redshift from NELs and deredshift the spectrum using the measured redshift. The spectrum is then normalized at  $3000 \text{ \AA}$ , rebinned into the same wavelength grids, and geometrically averaged bin by bin. The composite spectra are created from the low- $z$  quasar sample, and are shown in Fig. 7(a). Mg II BAL quasars are redder than the non-BAL quasars. The redness of Mg II BAL composite spectrum is due to the overall red SED instead of the BAL absorption troughs. To the first order approximation, the composite spectrum of Mg II BAL quasars is similar to the non-Mg II BAL quasars on both ultraviolet Fe II around Mg II,  $H\beta$ ,  $[\text{O II}]\lambda 3727$ ,  $[\text{Ne III}]\lambda 3869$ , and the red side of Mg II line profile, after de-reddening with an  $E(B - V) = 0.078$  for the SMC-like extinction curve (blue curve in the panel (a) of Fig. 7). This extinction value is similar to that obtained by Reichard et al. (2003b). However, there are subtle differences between the two composite spectra. The Mg II BAL composite spectrum shows stronger optical Fe II, but weaker  $[\text{Ne V}]\lambda 3425$  in comparison with non-Mg II BAL composite spectrum. A deficit of the Mg II flux in the Mg II BAL composite spectrum starts well from the redside of the Mg II line centroid. There is also excess emission in the  $H\beta$  wings in the Mg II BAL composite spectrum.

In order to look into more detail the spectrum of Mg II BAL quasars with different properties, we divide the sample into different bins according to their location on the continuum spectral-index versus  $[\text{O III}]$  equivalent width diagram (Fig. 5 panel (b)). A total six bins are adopted, each with a combination of blue ( $\beta_{[3K,4K]} \leq -2.2$ ), flat ( $-2.2 < \beta_{[3K,4K]} \leq -1.0$ ), red ( $\beta_{[3K,4K]} > -1.0$ ) in the spectral slope and  $[\text{O III}]$ -strong ( $EW_{[\text{O III}]} \geq 20 \text{ \AA}$ ) and  $[\text{O III}]$ -weak ( $EW_{[\text{O III}]} < 20 \text{ \AA}$ ). Composite spectra have been constructed separately for Mg II BAL and non-Mg II BAL quasars in each bin with proper number of sources. Because there are only two Mg II BAL quasars with  $\beta_{[3K,4K]} \leq -2.2$  in our sample, we will not show the result for Mg II BAL quasars in the blue bin. Similarly, only three Mg II BAL quasars fall in the bin with red and  $[\text{O III}]$ -strong spectrum, thus we will not consider this bin. As a result, only three composite BAL spectra are built. These composite spectra are shown in Fig. 7, while emission line parameters are measured and listed in Table 3.

By comparing the composite spectra of Mg II BAL quasars with different spectral indices and  $[\text{O III}]$  equivalent widths, we find: (1)  $[\text{O III}]$ -weak Mg II BAL quasars show a deficit in the

Mg II flux much larger and also extending to more redward than [O III]-strong Mg II BAL quasars. (2) Other NELs are also much weaker in the [O III]-weak Mg II BAL quasars. In particular, [Ne V] $\lambda$ 3424 is almost completely absent. However, when normalized to [O III], the narrow optical Fe II emission is much stronger. (3) The overall spectra of red and flat Mg II BAL quasars are very similar except for the continuum slope and some narrow line strength, which can be ascribed to a combination of the dust extinction plus a star-light contribution in the long-wavelength.

The non-Mg II BAL composite spectra have higher  $S/N$  ratios than their correspondent Mg II BAL composite spectra due to a large number of available spectra in each group. As in Mg II BAL quasars, the other NELs of [O III]-weak non-Mg II BAL quasars are weak as well, suggesting an overall weakness in narrow lines. Indeed, when normalized to [O III], the equivalent widths of narrow lines are similar for [O III]-weak and [O III]-strong objects, except for narrow Fe II lines. The former also displays stronger broad optical Fe II emission as already noticed in many previous works (e.g., Boroson & Green 1992, hereafter BG92). The equivalent widths of narrow lines increase from red to blue composite spectra for both [O III]-strong and [O III]-weak groups. Stellar absorption lines are visible in the composite of red quasars. The presence of prominent high order Balmer absorption lines suggests a recent starburst in the host galaxies. The differences in the red to blue sequences can be explained by increasing dust extinction from the red to blue sequences. As extinction to the nucleus increases, the continuum and broad lines dim more than narrow lines, resulting in an apparent increase in the equivalent width of NELs. Because both extinction and star-light contamination makes the spectrum redder, the equivalent width of [O II] increases more relative to [O III]. This is verified with the composite spectra (see also Table 3).

The Mg II BAL and non-Mg II BAL quasars in the [O III]-weak group have similar equivalent widths of [O III] and of broad  $H\beta$ . In the flat spectrum group, Mg II BAL quasars have stronger Balmer narrow lines and narrow optical Fe II component, weaker [Ne III], and much weaker [Ne V] than non-Mg II BAL quasars, but have a similar [O II] equivalent width. We find a similar behavior for the red spectrum group as well, in comparison with non-Mg II BAL quasars.

### 3.3. The Fraction of Mg II BAL Quasars

There are 68 Mg II BAL quasars in the low- $z$  quasar sample, which constitute 0.96% of the sample. After correcting for the missing and mis-classified BAL quasars introduced by  $\Delta v_c$  cut in  $AI$  discussed in §2.2, we find that the fraction of Mg II BAL quasars is  $F_{Mg\ II\ BAL} = 1.17\%$  in the SDSS quasars. This fraction may still under-estimate the true value slightly because Mg II BAL trough may fall outside of SDSS spectral coverage for some quasars with  $z \sim 0.4$ . This number is consistent with previous studies, which all yield a fraction of about 1% for Mg II BAL quasars based on the visual examination of C IV BAL quasars for the presence of strong Mg II absorption lines (Weymann et al. 1991; Boroson & Meyers 1992; Turnshek et al. 1997). More recently, Trump et al. (2006) found a fraction of 1.31% for broad Mg II BAL quasars in the SDSS DR3 quasars in the redshift range  $0.5 < z < 2.15$  that satisfied an  $AI$  definition of  $\Delta v_c = 1000\text{ km s}^{-1}$ . With their

definition, we found a slightly high value of 2.05%.

As we have shown, Mg II BAL quasars are usually redder than non-Mg II BAL quasars as a whole and this can be attributed to dust reddening in Mg II BAL quasars. Dust reddening will introduce two additional selection effects for Mg II BAL quasars. First, dust extinction will dim Mg II BAL quasars, and hence they tend to be missed in a magnitude limit quasar sample. Using the average extinction of 0.078 mag of SMC-like dust derived by the comparison of the composite spectra of Mg II BAL quasar and non-Mg II BAL quasars, we find that the average extinction correction to the  $i$ -band magnitude for loBAL quasars in the observed frame is between 0.25 and 0.33 mag for redshifts from 0.4 to 0.8. Because the quasar luminosity is fairly steep with a slope of -3.1 (Richards et al. 2003), this correction will introduce a factor of around 2. However, the fraction of Mg II BAL quasars missed due to extinction is sensitive not only to the average excess extinction, but also the extinction distribution. Using the average extinction will under-estimate the true fraction. Second, because most SDSS quasars in the redshift range of  $z \sim 0.4 - 0.8$  are selected via their colors and point-like morphologies, the reddening would move some quasars outside of color locus for quasar candidates, and the extinction to the nucleus also make the galaxy contribution more prominent, as such they might be missed due to their extend morphologies. Thus the corrected fraction of Mg II BAL quasars should be  $> 2\%$ .

Recent surveys in other bands have suggested that the number of optically-selected quasars will miss half of the total quasar population (Martinez-Sansigre et al. 2005; Alonso-Herrero et al. 2006; Stern et al. 2007), but most of the missed quasars may be type-2 rather than type-1, thus may not significant affect the fraction of Mg II BAL quasars. Dust-reddened quasars missed in optical surveys have been found in other non-optical surveys, such as hard X-ray surveys (Polletta et al. 2007), infrared surveys (Cutri et al. 2001; Lacy et al. 2004; Glikman et al. 2004, 2007) and radio surveys (White et al. 2003). It has been suggested that the fraction of loBAL quasars are much higher among those dust reddened quasars, e.g., 32% (Urrutia et al. 2008). A pilot study of near-infrared bright quasar candidates from UKDISS suggests that the reddening quasars missed by SDSS probably accounts no more than 30% (Maddox et al., 2008; cf Glikman et al. 2007). From these multiband observation, the upper limit of the Mg II BAL fraction is estimated to be  $< 7\%$ . To summarize, the fraction of Mg II BAL quasars is from 2% to 7%.

It was suggested that BAL quasar fraction increases with continuum luminosity (Ganguly et al. 2007). However, G09 pointed out that  $S/N$  and luminosity are degenerate, and it is unclear if BAL quasars are truly more luminous or are simply identified at higher  $S/N$ . To examine whether such a luminosity dependent trend is also seen in loBAL quasars, and break the degeneracy of the  $S/N$ -luminosity dependence, we split our sample into low and high luminosity groups. The division line is so chosen that the two group has the same size. The average luminosities for the low and high groups are  $\lambda L_{\lambda}(5100\text{\AA}) = 2.8 \times 10^{44}$  and  $\lambda L_{\lambda}(5100\text{\AA}) = 8.8 \times 10^{44}$  erg s $^{-1}$ , respectively. We further divide the sample into three equal size  $S/N$  bins, and calculate the loBAL fraction in each bin. The results are shown in the left panel of Fig. 8. For comparison, we also show the result of the whole sample. As one can see, the fraction of Mg II BAL quasars decreases with decreasing

median spectral  $S/N$  ratios, from 1.7% for  $S/N \sim 25$  to 0.8% for  $S/N \sim 15$  for the whole sample. A similar trend is also seen in the high luminosity group. However, the increase can be solely due to luminosity effect because quasars in the highest  $S/N$  ratio bin are a factor of two more luminous than its neighbor bin even for the high luminosity group. The constancy of BAL fraction  $7 < S/N < 15$  is an indication that  $S/N$  ratio does not actually matter. For a given  $S/N$  ratio, the BAL fraction in high luminosity group is twice of that in low luminosity group.

However, in each  $S/N$  bin, there is still a variation of  $S/N$ . In order to break the degeneracy, we try to use logistic regression (e.g., Fox 1997) to assess how the likelihood of a quasar being classified as BAL or non-BAL quasars depends on the luminosity at  $5100\text{\AA}$  and/or  $S/N$ . Logistic regression solves for the natural logarithm of the odd ratio in terms of the variables as follows:

$$\ln \frac{Pr(G = 1|L, S/N)}{Pr(G = 2|L, S/N)} = \beta_0 + \beta_1 \ln(S/N) + \beta_2 \ln(\lambda L_\lambda(5100\text{\AA})/10^{44}) \quad (7)$$

where  $G = 1$  when a quasar is classified as BAL and  $G = 2$  as non-BAL. The logit as the logarithm of the ratio of the probabilities, is just the logarithm of the BAL to non-BAL ratio. The coefficients are calculated using the Newton-Raphson method, and errors are estimated by bootstrapping. We calculated the standard deviation of the coefficients with 1000 random subsets of the true data. In the Monte-Carlo simulation, we simulate the continuum subtracted spectrum around Mg II regime using the error array provided by the SDSS pipeline, and remeasure the absorption line parameters as for the real spectrum, i.e., reclassify as BAL or non-BAL quasars, for each object. The continuum luminosity is generated using the model parameters and their uncertainties. The uncertainty in the  $S/N$  ratio is very small and is not considered. We obtain  $\beta_0 = -4.42 \pm 0.74$ ,  $\beta_1 = -0.78 \pm 0.48$  and  $\beta_3 = 1.37 \pm 0.32$ . In other words, the fraction of Mg II BAL decreases with  $S/N$  at  $1.6\sigma$  significance and increases with luminosity at  $4.3\sigma$  significance. Therefore, the analysis supports that luminosity is a far more important factor in determining the BAL fraction while it is far less affected by the  $S/N$  ratio. We show in the right panel of Fig. 8  $F_{Mg\ II\ BAL}$  as a function of the luminosity. Our results strongly suggest that Mg II BAL quasars are averagely more luminous than non-Mg II BAL quasars, consistent with Ganguly et al. (2007). G09 did not find such trend in their sample. The difference may be due to a relatively larger luminosity range of our sample than G09 or that Mg II BAL quasars depend more strongly on quasar luminosity than HiBAL quasars.

Fig. 9 shows  $F_{Mg\ II\ BAL}$  as a function of  $EW_{[O\ III]}\lambda 5007$ , the equivalent width of [O III]  $\lambda 5007$ . The fraction decreases from 1.65% at  $EW_{[O\ III]} = 8.6\ \text{\AA}$  to 0.51% at  $EW_{[O\ III]} = 34.3\ \text{\AA}$ . Because both  $F_{Mg\ II\ BAL}$  and  $EW_{[O\ III]}$  are correlated with optical luminosity (Dietrich et al. 2002), there is a concern that such a dependence is caused by luminosity effect. In order to break the degeneracy, we split the sample into two luminosity bins. Both the high and low luminosity bins show the same trend with a higher overall fraction and steep slope for high luminosity bin, thus dependence of Mg II BAL fraction on [O III]-strength is not a secondary effect of luminosity.

Boroson (2002) argued that BAL quasars occupy the high Eddington ratio and the black hole mass locus on the Eddington ratio versus black hole mass diagram. Ganguly et al. (2007) found that the frequency and properties of BALs depend on both black hole mass and Eddington ratio

for their sample of HiBAL quasars. We also investigate the possible dependence of  $F_{Mg II BAL}$  on  $M_{BH}$  and  $L/L_{Edd}$ . We divided our quasars into three bins in either Eddington ratio or black hole mass, and calculate  $F_{Mg II BAL}$  in each bin. We find that  $F_{Mg II BAL}$  in the highest Eddington ratio bin ( $L/L_{Edd} \geq 0.24$ ) is significantly higher (two times) than that in rest of the two bins, the difference is more than  $2.6\sigma$  (Fig. 10). However, we do not find any significant correlation between  $F_{Mg II BAL}$  and  $M_{BH}$ , in the range from a few  $10^7$  to  $10^9 M_{\odot}$  in our sample. In passing, we note that using other formalisms of black hole mass estimate based on broad  $H\beta$  line (e.g., Kaspi et al. 2000; Green & Ho 2005; Wang et al. 2009) yields the same conclusion.

### 3.4. Emission Line Properties of Mg II BAL Quasars

Based on a small sample of infrared selected quasars, Boroson & Meyers (1992) proposed that Mg II BAL or loBAL quasars have very weak even undetectable [O III] emission compared to non-loBAL quasars. In their sample, the [O III] equivalent widths of loBAL quasars are typically less than 5 Å. As discussed in the last section, we find that there are still a fraction of loBAL quasars with a relatively high [O III] equivalent width, though the fraction of Mg II BAL quasars in the [O III]-strong sample is only one-third of that in the [O III]-weak sample. Only 20 of 68 Mg II BAL quasars have their  $EW_{[O III]}$  smaller than 5 Å, while 13 Mg II BAL quasars have higher than 20 Å, some of them have even higher than 100 Å. We compare the properties of [O III]-strong and [O III]-weak Mg II BAL quasars, and find significant difference between the two types (Table 3). First, [O III]-strong loBAL quasars show much weaker Mg II absorption feature (Fig. 7 (b)). The median value of  $AI$  is 631 km s<sup>-1</sup> in the [O III]-strong loBAL sub-sample, while the median value of  $AI$  is 1141 km s<sup>-1</sup> in [O III]-weak loBAL sub-sample. Second, [O III]-weak loBAL quasars also display systematically weaker broad  $H\beta$  line as shown in Fig 7 (b). Third, [O III]-weak loBAL quasars have strong UV and optical Fe II emission, and a stronger narrow component of Fe II, in particular. The median  $EW_{UV Fe II}$  are  $136.01_{-3.99}^{+12.79}$  Å and  $113.6_{-1.38}^{+2.64}$  Å for [O III]-weak and [O III]-strong loBAL quasars, respectively. The intensity ratio of broad optical Fe II component to broad  $H\beta$  component in the [O III]-weak loBAL composite spectrum is twice as strong as that in the [O III]-strong BAL composite spectrum, and the intensity ratio of Fe II narrow component to [O III] is more than 20 times larger in the former.

In order to find the connection between the outflow and emission line region, we explore the correlation between the outflow parameters and emission line parameters. We find that  $AI$  is marginally correlated with UV Fe II (with a Spearman rank correlation coefficient of  $r_s = 0.27$  and a null hypothesis probability of  $P_r = 0.05$ ) in the sense that there is an upper envelope of  $AI$ , which increases with  $EW_{Fe II UV}$  (Fig.11 (a)). As shown in Fig.11 (b), there seems also an upper border in the  $AI$  for a given  $EW_{[O III]}$ , which decreases with  $EW_{[O III]}$  and there seems also a low boundary for  $AI$ .  $AI$  is marginally anti-correlated  $EW_{[O III]}$  with  $r_s = -0.24$  and  $P_r = 0.07$ . Apparently, larger sample are required to confirm these weak trends.

### 3.5. Properties of Intermediate Width Mg II Absorption Line Quasars

In §2.2, we defined our criteria of Mg II BAL quasars by comparing the frequency of C IV BAL with  $AI(\Delta v_c \geq 2000) > 0$  at different cuts in  $\Delta v_c$  of Mg II absorption lines. We finally choose a contiguous absorption with a minimum depth of 10% of the intrinsic emission spectrum over a width  $\Delta v_c = 1600 \text{ km s}^{-1}$ . With this definition, we can identify BAL quasars with Mg II absorption lines that are associated with BALs. Note that Trump et al. (2006) and some other previous works have used  $1000 \text{ km s}^{-1}$  as the selection criteria for loBAL quasars. If quasars with absorption width between  $1000 \text{ km s}^{-1}$  and  $1600 \text{ km s}^{-1}$  are true Mg II BAL, they should have similar properties in the emission lines and continuum as these selected with  $\Delta v_c = 1600 \text{ km s}^{-1}$ . In the following, we will check whether there is a clear distinction in the Mg II absorbers with a width above and below  $1600 \text{ km s}^{-1}$ .

In our low- $z$  quasar sample, there are 68 Mg II BAL quasars with  $\Delta v_c \geq 1600 \text{ km s}^{-1}$ , and 76 quasars with  $1000 \leq \Delta v_c < 1600 \text{ km s}^{-1}$  (hereafter lowV group). We compare continuum and emission line properties of these two groups with non-Mg II BAL quasars as well as between the two groups either statistically or using their composite spectra. Table 3 summarizes the emission line parameters measured from the composite spectrum of lowV quasars. We find that the emission line properties, including Fe II, [Ne V] and [O III] of lowV quasars are similar to non-Mg II BAL quasars, but different from BAL quasars. However, the composite spectrum of lowV group is significantly redder than that of non-Mg II BAL quasars.

We also measure the parameters of broad and narrow optical emission lines and continuum, including  $H_\beta$  profile, the equivalent width of UV Fe II and [Ne V], FWHM of [O III] and [O II],  $\lambda L_\lambda(5100\text{\AA})$  and  $\beta_{[3K,4K]}$  for each quasar. Fig. 12 shows the distributions of line and continuum parameters for the two samples of Mg II absorbers as well as that of non-Mg II BAL quasars. Significant difference between lowV quasars and Mg II BAL quasars is found in distributions of following parameters: the equivalent width of UV Fe II, [Ne V] and  $\lambda L_\lambda(5100\text{\AA})$ , as shown in Fig.12. Kolmogorov-Smirnov (KS) test gives null probabilities of  $9 \times 10^{-3}$ ,  $6 \times 10^{-3}$  and  $6 \times 10^{-5}$ , respectively, for UV Fe II, [Ne V] and  $\lambda L_\lambda(5100\text{\AA})$ , that their distributions are drawn from the same parent population for lowV and Mg II BAL quasars. Mg II BAL quasars have weaker [Ne V] and [O II], stronger optical Fe II and higher observed optical luminosity than lowV quasars. The two groups have almost the same distributions in continuum slope. The lowV quasars show the similar distributions of all emission line parameters as non-Mg II BAL quasars, except for a redder continuum and lower observed optical luminosities.

## 4. Summary and Discussion

We have selected 68 Mg II BAL quasars from the SDSS spectroscopic quasar sample with a redshift of  $0.4 < z \leq 0.8$  and a median  $S/N \geq 7$  using criteria of a continuous absorption over a velocity interval greater than  $1600 \text{ km s}^{-1}$  for a depth of at least 10%. The BAL-selected criterion

is a trade-off between the completeness and consistency with respect to the canonical definition of BAL quasars that have the 'balnicity index'  $BI > 0$  in C IV BAL. We adopted such a criterion to ensure that  $\sim 90\%$  of our sample are classical BAL quasars and the completeness is  $\sim 80\%$ , based on extensive tests using high- $z$  quasar samples with measurements of both C IV and Mg II BALs. The low- $z$  sample is used to define the fraction of Mg II BAL quasars and its dependence on the continuum and emission line properties, the difference between Mg II and non-Mg II BAL quasars. We find that, (1) the fraction of Mg II BAL quasars in the optical survey is around 1.2%. The fraction does not include correction for internal dust extinction of BAL quasars and the color bias against reddened loBAL quasars. After correcting these factors, the true Mg II BAL fraction is likely in between 2% and 7%. (2) Mg II BAL quasars are more frequently found in quasars with low [O III] equivalent width and high continuum luminosity although they show a wide range of [O III] equivalent width. loBAL quasars display stronger narrow optical Fe II emission lines and UV Fe II emission, weaker even absent [Ne V] lines. (3) The fraction of quasars with Mg II BAL increases strongly with the Eddington ratio but does not correlate with the black hole mass. (4) There is an excess of intrinsic reddening in Mg II BAL quasars and quasars with intermediate width Mg II absorption lines with an average of 0.08 mag for SMC-like dust grain. In this section, we will discuss the implication of our results.

It is generally believed that NELs are nearly isotropic in quasars because they are produced in an extended region. In contrast the BEL region and continuum are thought to be much more compact and can be blocked on some lines of sight by obscuration (e.g., Antonucci 1993). The excess extinction in Mg II BAL quasars with respect to non-Mg II BAL quasars will enhance the conclusion that [O III] equivalent width is lower in loBAL quasars. The conclusion will be further strengthened if we consider the anisotropic emission of optical continuum from the accretion disk because it is generally believed that BAL quasars are seen nearly edge-on. The large range of observed  $EW_{[O III]}$  among Mg II BAL quasars suggests that loBAL occurs in both [O III]-weak and [O III]-strong emission quasars, but the covering factor decreases strongly as the [O III] strength increases.

If [O III] is considered as an indicator of overall strength of NELs, the strength of other lines relative to [O III] should connect more to the physical state of narrow-line region (NLR) or ionizing continuum. The absence of [Ne V] in [O III]-weak Mg II BAL turns out to be a rather surprise. Previous studies have suggested that [Ne V] is produced in the high density, inner NLR (e.g., Heckman et al. 1981; De Robertis & Osterbrock 1984; Whittle 1985a, 1985b). Lack of [Ne V] emission indicates that there is no such region or the inner NLR does not expose to a hard ionizing continuum. Interaction of BAL outflow with inner NLR may destroy dense clouds in the inner NLR. However, the presence of strong narrow optical Fe II emission would suggest such dense inner NLR does exist but with low ionization parameters (see Véron-Cetty et al. 2004; also Wang, Dai & Zhou 2008). Then we look at the option that the NLR only sees a soft ionizing continuum. BAL quasars, loBAL quasars in particular, are weak in soft X-rays (Green et al. 1995; Brinkmann et al. 1999), which are required to produce  $Ne^{4+}$  (ionization potential 97 eV). If NLR sees a continuum similar



to the observed one, the absence of [Ne V] can be naturally explained. Because the weakness of soft X-rays in BAL quasars is usually attributed to X-ray absorption rather than intrinsic weakness (Wang et al. 1999; Gallagher et al. 1999, 2002), this requires that the [Ne V] emission region is behind the X-ray absorber. There are two possibilities for this, the outflow has a large covering factor or [Ne V] emission region located coincidentally behind the outflow. Nagao et al. (2001) proposed that [Ne V] emission region is the inner region of the dust torus, and use the hypothesis to explain the unification of two type Seyfert galaxies. In their scenarios, [Ne V] emission region lies on the equatorial plane, which is coincident with the region shielded by disk wind.

In order to check this, we select 250 non-Mg II BAL quasars with  $S/N > 20$ ,  $\beta_{[3K,4K]} > -2.2$  and  $EW_{[O III]} < 20$ , out of which 119 quasars do not show detectable [Ne V] emission line in the spectra. Fig. 13 shows the two composite spectra of these non-Mg II BAL quasars with/without [Ne V] emission, the emission parameters are shown in Table 3. The composite spectrum of the 119 non-BAL quasars without [Ne V] is similar to that of Mg II BAL quasars, showing stronger optical narrow Fe II emission, weak [O III] strength and strong UV Fe II but with a blue continuum. These quasars are probably from the same parent population of loBAL quasars but our line of sight does not intersect the outflow. The high fraction of non-BAL quasars without [Ne V] emission line indicates that the covering factor of loBALR is not large.

Several observed trends may be explained by the strong correlation between the frequency of loBAL and Eddington ratio, and the correlations of the Eddington ratio with the other parameters concerned. It was reported that narrow optical Fe II strength is fairly well correlated with the Eddington ratio for low redshift quasars (Dong et al. 2009b). Dietrich et al. (2002) demonstrated that [O III] strength is inversely correlated with the Eddington ratio for quasars. Weakness of Mg II in the red-side of Mg II line profile is difficult to be ascribed to the absorption, and can be understood in this context as well via a fairly strong anti-correlation between EW of Mg II and the Eddington ratio (Dong et al. 2009a). Thus, the Eddington ratio can be an underlying driver for the different covering factor of low ionization BALR. We note that even in the highest Eddington ratio bin, the fraction of loBAL quasars is only a factor of 2 of the value in the rest two low Eddington ratio bins. There is no correlation between the fraction of loBAL with black hole mass for this sub-sample. Narrow line Seyfert 1 galaxies (NLS1s) are believed to be the low mass counter-parts of high accretion rate quasars. Zhou et al. (2006a; 2006b) found that several NLS1s also show Mg II BALs. Twelve of our low- $z$  Mg II BAL quasars can be formally classified as NLS1s according to the formal criterion of  $H\beta < 2000 \text{ km s}^{-1}$ , which account for 1.6% of NLS1s in this redshift range. Therefore, NLS1s do not appear to show significantly different properties from other quasars with similar optical luminosity. The black hole mass range of these loBAL-NLS1s is very narrow with  $[2.1, 7.8] \times 10^7 M_{\odot}$ . It is possible that black hole mass does not matter once it is above certain threshold.

Finally, most quasars with Mg II BALs or intermediate width Mg II absorption lines show reddened colors. We already noticed that the two group quasars show significantly different properties of emission lines, and the BAL fraction among the latter group is less than 25% (refer §2.2). Thus,

it is unlikely due to mixing of un-identified BAL quasars. The ubiquity of dust in intermediate and LoBAL outflows may be naturally explained as both absorbers are large scale outflows (e.g., Dunn et al. 2010). The presence of dust will significantly boost the radiative force and thus it allow gas in a relative large distance from the nucleus to be accelerated by the quasar radiation. In other word, gas free from dust will not be accelerated to high velocity by radiation pressure. In this case, dust reddening would be preferably observed in the outflow direction. As we have argued that [Ne V]-weak quasars may be Mg II BAL quasars seen from an off-BALR direction, and their color can be fairly blue, thus dust may not present in other direction. This is consistent with above argument. Certainly, critical test for this can be done with a comparative study of broad band infrared SED of BAL and non-BAL quasars.

Dust reddening is ubiquitous in broad ( $\Delta v_c \geq 1000 \text{ km s}^{-1}$ ) Mg II absorbers, regardless of whether they are BAL or non-BAL quasars. The average excess reddening is  $E(B-V) \sim 0.08 \text{ mag}$  for SMC-type dust for both groups. However, we think that the intermediate width Mg II absorption quasars might have somewhat lower reddening than Mg II BAL quasars. Because quasars with large extinction, more likely BAL quasars, are missed in the SDSS quasar sample due to color selection criteria of quasar target, this sample explores only the relative low extinction end of quasars. Thus the similar color distribution for quasars with Mg II BAL and with intermediate width Mg II absorption lines may be caused by the color selection effect that introduces a truncation in the severely reddened quasars. Indeed, radio and infrared-selected Mg II BAL quasars show much larger extinction with  $E(B-V)$  up to 1.5 mag (Urrutia et al. 2008), while there is no good statistical work for intermediate width Mg II. So it is not conclusive whether Mg II BAL quasars and quasars with intermediate width Mg II absorption lines have similar dust extinctions.

This work has made use of the data obtained by SDSS. Funding for the SDSS and SDSS-II has been provided by the Alfred P. Sloan Foundation, the Participating Institutions, the National Science Foundation, the U.S. Department of Energy, the National Aeronautics and Space Administration, the Japanese Monbukagakusho, the Max Planck Society, and the Higher Education Funding Council for England. The SDSS Web Site is <http://www.sdss.org/>.

The SDSS is managed by the Astrophysical Research Consortium for the Participating Institutions. The Participating Institutions are the American Museum of Natural History, Astrophysical Institute Potsdam, University of Basel, University of Cambridge, Case Western Reserve University, University of Chicago, Drexel University, Fermilab, the Institute for Advanced Study, the Japan Participation Group, Johns Hopkins University, the Joint Institute for Nuclear Astrophysics, the Kavli Institute for Particle Astrophysics and Cosmology, the Korean Scientist Group, the Chinese Academy of Sciences (LAMOST), Los Alamos National Laboratory, the Max-Planck-Institute for Astronomy (MPIA), the Max-Planck-Institute for Astrophysics (MPA), New Mexico State University, Ohio State University, University of Pittsburgh, University of Portsmouth, Princeton University, the United States Naval Observatory, and the University of Washington.

## REFERENCES

- Alonso-Herrero, A., et al. 2006, *ApJ*, 640, 167
- Antonucci, R. 1993, *ARA&A*, 31, 473
- Becker, R. H., White, R. L., Gregg, M. D., Brotherton, M. S., Laurent-Muehleisen, S. A., & Arav, N. 2000, *ApJ*, 538, 72
- Boroson, T. A. 2002, *ApJ*, 565, 78
- Boroson, T. A., & Green, R. F. 1992, *ApJS*, 80, 109
- Boroson, T. A., & Meyers, K. A. 1992, *ApJ*, 397, 442
- Brandt, W. N., Laor, A., & Wills, B. J. 2000, *ApJ*, 528, 637
- Brinkmann, W., Wang, T., Matsuoka, M., & Yuan, W. 1999, *A&A*, 345, 43
- Brotherton, M. S., Tran, H. D., Becker, R. H., Gregg, M. D., Laurent-Muehleisen, S. A., & White, R. L. 2001, *ApJ*, 546, 775
- Brotherton, M. S., De Breuck, C., & Schaefer, J. J. 2006, *MNRAS*, 372, L58
- Cohen, M. H., Ogle, P. M., Tran, H. D., Vermeulen, R. C., Miller, J. S., Goodrich, R. W., & Martel, A. R. 1995, *ApJ*, 448, L77
- Cutri, R. M., Nelson, B. O., Kirkpatrick, J. D., Huchra, J. P., & Smith, P. S. 2001, *Bulletin of the American Astronomical Society*, 33, 829
- Dai, X., Shankar, F., & Sivakoff, G. R. 2008, *ApJ*, 672, 108
- De Robertis, M. M., & Osterbrock, D. E. 1984, *ApJ*, 286, 171
- Dietrich, M., Hamann, F., Shields, J. C., Constantin, A., Vestergaard, M., Chaffee, F., Foltz, C. B., & Junkkarinen, V. T. 2002, *ApJ*, 581, 912
- Dong, X.-B., Wang, T.-G., Wang, J.-G., Fan, X., Wang, H., Zhou, H., & Yuan, W. 2009a, *ApJ*, 703, L1
- Dong, X., Wang, J., Wang, T., Wang, H., Fan, X., Zhou, H., & Yuan, W. 2009b, *arXiv:0903.5020*
- Dong, X., Wang, T., Wang, J., Yuan, W., Zhou, H., Dai, H., & Zhang, K. 2008, *MNRAS*, 383, 581
- Dunn, J. P., et al. 2010, *ApJ*, 709, 611
- Egami, E., Iwamuro, F., Maihara, T., Oya, S., & Cowie, L. L. 1996, *AJ*, 112, 73
- Fan, L. L., Wang, H. Y., Wang, T., Wang, J., Dong, X., Zhang, K., & Cheng, F. 2009, *ApJ*, 690, 1006

- Fitzpatrick, E. L. 1999, *PASP*, 111, 63
- Forster, K., Green, P. J., Aldcroft, T. L., Vestergaard, M., Foltz, C. B., & Hewett, P. C. 2001, *ApJS*, 134, 35
- Fox, J. 1997, *Applied Regression Analysis, Linear Models, and Related Methods* (Thousand Oaks, CA: Sage Publications), 438
- Gallagher, S. C., Brandt, W. N., Chartas, G., & Garmire, G. P. 2002, *ApJ*, 567, 37
- Gallagher, S. C., Brandt, W. N., Chartas, G., Priddey, R., Garmire, G. P., & Sambruna, R. M. 2006, *ApJ*, 644, 709
- Gallagher, S. C., Brandt, W. N., Sambruna, R. M., Mathur, S., & Yamasaki, N. 1999, *ApJ*, 519, 549
- Gallagher, S. C., Hines, D. C., Blaylock, M., Priddey, R. S., Brandt, W. N., & Egami, E. E. 2007, *ApJ*, 665, 157
- Ganguly, R., & Brotherton, M. S. 2008, *ApJ*, 672, 102
- Ganguly, R., Brotherton, M. S., Cales, S., Scoggins, B., Shang, Z., & Vestergaard, M. 2007, *ApJ*, 665, 990
- Ghosh, K. K., & Punshly, B. 2007, *ApJ*, 661, L139
- Gibson, R. R., et al. 2009, *ApJ*, 692, 758
- Glikman, E., Gregg, M. D., Lacy, M., Helfand, D. J., Becker, R. H., & White, R. L. 2004, *ApJ*, 607, 60
- Glikman, E., Helfand, D. J., White, R. L., Becker, R. H., Gregg, M. D., & Lacy, M. 2007, *ApJ*, 667, 673
- Goodrich, R. W., & Miller, J. S. 1995, *ApJ*, 448, L73
- Green, P. J., et al. 1995, *ApJ*, 450, 51
- Greene, J. E., & Ho, L. C. 2005, *ApJ*, 630, 122
- Hall, P. B., et al. 2002, *ApJS*, 141, 267
- Hamann, F., & Ferland, G. 1993, *ApJ*, 418, 11
- Hewett, P. C., & Foltz, C. B. 2003, *AJ*, 125, 1784
- Hines, D. C., & Wills, B. J. 1995, *ApJ*, 448, L69
- Jiang, D. R., & Wang, T. G. 2003, *A&A*, 397, L13

- Kaspi, S., Smith, P. S., Netzer, H., Maoz, D., Jannuzi, B. T., & Giveon, U. 2000, *ApJ*, 533, 631
- Knigge, C., Scaringi, S., Goad, M. R., & Cottis, C. E. 2008, *MNRAS*, 386, 1426
- Konigl, A., & Kartje, J. F. 1994, *ApJ*, 434, 446
- Korista, K. T., et al. 1993, *ApJ*, 413, 445
- Lacy, M., et al. 2004, *ApJS*, 154, 166
- Maddox, N., & Hewett, P. C. 2008, *Memorie della Societa Astronomica Italiana*, 79, 1117
- Maddox, N., Hewett, P. C., Warren, S. J., & Croom, S. M. 2008, *MNRAS*, 386, 1605
- Martínez-Sansigre, A., Rawlings, S., Lacy, M., Fadda, D., Marleau, F. R., Simpson, C., Willott, C. J., & Jarvis, M. J. 2005, *Nature*, 436, 666
- Nagao, T., Murayama, T., & Taniguchi, Y. 2001, *PASJ*, 53, 629
- Ogle, P. M., Cohen, M. H., Miller, J. S., Tran, H. D., Goodrich, R. W., & Martel, A. R. 1999, *ApJS*, 125, 1
- Polletta, M., et al. 2007, *ApJ*, 663, 81
- Reichard, T. A., et al. 2003a, *AJ*, 125, 1711
- Reichard, T. A., et al. 2003b, *AJ*, 126, 2594
- Richards, G. T., et al. 2003, *AJ*, 126, 1131
- Sanders, D. B., Soifer, B. T., Elias, J. H., Neugebauer, G., & Matthews, K. 1988, *ApJ*, 328, L35
- Schlegel, D. J., Finkbeiner, D. P., & Davis, M. 1998, *ApJ*, 500, 525
- Schmidt, G. D., & Hines, D. C. 1999, *ApJ*, 512, 125
- Schneider, D. P., et al. 2007, *AJ*, 134, 102
- Skrutskie, M. F., et al. 2006, *AJ*, 131, 1163
- Stern, D., et al. 2007, *ApJ*, 663, 677
- Tolea, A., Krolik, J. H., & Tsvetanov, Z. 2002, *ApJ*, 578, L31
- Trump, J. R., et al. 2006, *ApJS*, 165, 1
- Turnshek, D. A., Monier, E. M., Sirola, C. J., & Espey, B. R. 1997, *ApJ*, 476, 40
- Urrutia, T., Lacy, M., & Becker, R. H. 2008, *ApJ*, 674, 80

- Vanden Berk, D. E., et al. 2001, *AJ*, 122, 549
- Véron-Cetty, M.-P., Joly, M., & Véron, P. 2004, *A&A*, 417, 515
- Vestergaard, M., & Peterson, B. M. 2006, *ApJ*, 641, 689
- Vestergaard, M., & Wilkes, B. J. 2001, *ApJS*, 134, 1
- Voit, G. M., Weymann, R. J., & Korista, K. T. 1993, *ApJ*, 413, 95
- Wang, J., Jiang, P., Zhou, H., Wang, T., Dong, X., & Wang, H. 2008a, *ApJ*, 676, L97
- Wang, T., Dai, H., & Zhou, H. 2008b, *ApJ*, 674, 668
- Wang, T. G., Wang, J. X., Brinkmann, W., & Matsuoka, M. 1999, *ApJ*, 519, L35
- Wang, H.-Y., Wang, T.-G., & Wang, J.-X. 2005, *ApJ*, 634, 149
- Wang, J.-G., et al. 2009, *ApJ*, 707, 1334
- Weymann, R. J. 2002, *Mass Outflow in Active Galactic Nuclei: New Perspectives*, 255, 329
- Weymann, R. J., Morris, S. L., Foltz, C. B., & Hewett, P. C. 1991, *ApJ*, 373, 23
- White, R. L., Helfand, D. J., Becker, R. H., Gregg, M. D., Postman, M., Lauer, T. R., & Oegerle, W. 2003, *AJ*, 126, 706
- Whittle, M. 1985a, *MNRAS*, 213, 1
- Whittle, M. 1985b, *MNRAS*, 216, 817
- Willott, C. J., Rawlings, S., & Grimes, J. A. 2003, *ApJ*, 598, 909
- York, D. G., et al. 2000, *AJ*, 120, 1579
- Zhou, H., Wang, T., Wang, H., Wang, J., Yuan, W., & Lu, Y. 2006a, *ApJ*, 639, 716
- Zhou, H., Wang, T., Yuan, W., Lu, H., Dong, X., Wang, J., & Lu, Y. 2006b, *ApJS*, 166, 128

Table 1. Different Definition for the BAL Quasars

	$v_l$	$v_u$	$\Delta v_c$	Reference
<i>BI</i>	3,000	25,000	2,000	Weymann et al. 1991 Tolea et al. 2002 Reichard et al. 2003a Trump et al. 2006 G09
<i>BI</i>	0	25,000	1,000	Reichard et al. 2003a
<i>BI</i> <sub>0</sub>	0	25,000	2,000	G09
<i>AI</i>	0	25,000	450	Hall et al. 2002
<i>AI</i>	0	29,000	1,000	Trump et al. 2006
<i>AI</i>	0	20,000	1,600	This work

Table 2. Low- $z$  Mg II BAL Quasars Catalog in SDSS DR5

Name <sup>a</sup>	R.A. J2000	Decl. J2000	Redshift	AI km s <sup>-1</sup>	$depth_{max}^b$	$V_{max}^c$ km s <sup>-1</sup>	$V_{min}^d$ km s <sup>-1</sup>	$V_{ave}^e$ km s <sup>-1</sup>	$\lambda L_{\lambda}(5100\text{\AA})$ 10 <sup>44</sup> erg s <sup>-1</sup>	$\beta_{[3K,4K]}$	$EW_{[O III]}$ Å	$EW_{[N e V]}$ Å	$M_{BH}$ 10 <sup>8</sup> M <sub>⊙</sub>	$L/L_{EDD}$	
010352.46+003739.7	15.968604	0.627704	0.7031	480± 1	0.73	11500	9100	10280	22.	-1.21	15.1	0.6	16.	0.097	
023102.49-083141.2	37.760410	-8.528133	0.5868	303± 2	0.72	3750	2100	2966	3.5	-2.04	18.5	0.9	2.1	0.12	
025026.66+000903.4	42.611093	0.150945	0.5963	1032± 8	0.32	3400	750	2066	5.4	0.99	24.2	3.6	37.	0.010	
080934.64+254837.9	122.394340	25.810552	0.5454	519± 1	0.49	1600	0	665	9.2	-2.11	13.4	0.4	18.	0.036	
081655.34+074311.5	124.230604	7.719886	0.6442	312± 2	0.75	5500	3750	4703	5.7	-1.52	18.1	3.9	2.6	0.15	
082231.53+231152.0	125.631381	23.197803	0.6530	677± 1	0.42	2350	450	1346	18.	-1.62	51.0	2.2	50.	0.027	
083525.98+435211.2	128.858253	43.869796	0.5678	781± 2	0.66	20000	16250	18120	13.	-1.58	4.3	0.0	6.0	0.16	
083613.23+280512.1 <sup>†</sup>	129.055150	28.086698	0.7412	4105± 11	0.30	17050	5800	10546	5.3	-1.51	7.0	0.0	0.73	0.52	
084716.04+373218.0	131.816838	37.538359	0.4539	347± 2	0.73	4100	2400	3265	3.5	-2.22	156.6	4.5	0.98	0.26	
085215.66+492040.8	133.065270	49.344685	0.5664	1143± 4	0.14	2250	0	1202	4.3	-1.50	10.7	0.7	4.1	0.076	
085357.87+463350.6	133.491147	46.564063	0.5497	418± 1	0.62	4400	2800	3642	8.2	-1.47	3.5	0.2	6.2	0.095	
091146.06+403501.1 <sup>†</sup>	137.941942	40.583652	0.4412	1053± 7	0.33	6100	3150	4082	2.9	-0.09	21.2	2.4	0.41	0.51	
092157.62+103539.0 <sup>†</sup>	140.490091	10.594188	0.5476	1730± 8	0.49	8950	3250	6068	2.7	-1.61	7.4	0.5	0.33	0.58	
092928.63+324129.9	142.369302	32.691639	0.7748	279 ± 2	0.79	9900	8050	8997	1.3	-1.78	9.3	0.2	5.3	0.18	
093034.79+570520.7	142.644964	57.089097	0.6374	314 ± 2	0.72	10350	8750	9493	6.8	-2.00	7.1	0.0	1.7	0.29	
094443.13+062507.4	146.179709	6.418734	0.6951	1532± 1	0.48	9300	4300	7245	69.	-1.42	2.9	0.0	18.	0.28	
101203.31+492148.2	153.013803	49.363391	0.7389	1030± 3	0.56	7650	700	4029	8.5	-1.73	1.1	0.0	15.	0.041	
102021.21+121909.1	155.088391	12.319199	0.4793	3320± 17	0.31	18350	0	11309	4.0	-0.05	2.4	0.0	1.0	0.28	
102802.32+592906.6	157.009676	59.485190	0.5349	995± 3	0.36	2650	300	1421	2.5	-2.11	7.1	0.9	2.5	0.072	
102839.11+450009.4	157.162961	45.002620	0.5826	773± 1	0.41	2450	100	1204	24.	-1.41	11.8	0.0	24	8.9	0.20
103621.60+393701.6	159.090011	39.617129	0.7997	777± 1	0.48	3100	200	1488	40.	-1.31	5.0	0.0	48.	0.059	
104210.43+501609.2	160.543497	50.269224	0.7873	1384± 1	0.13	3650	1050	2503	20.	-2.23	1.1	1.8	21.	0.070	
104459.60+365605.1	161.248363	36.934775	0.7015	3578± 2	0.02	17650	800	6311	42.	-1.34	1.7	0.0	9.1	0.33	
105259.99+065358.1 <sup>†</sup>	163.249983	6.899474	0.7224	2508± 7	0.53	12900	4600	8792	8.9	-1.27	9.8	0.0	0.69	0.92	
112632.81+430938.6	171.636726	43.160726	0.4356	886± 3	0.24	1800	0	874	6.2	-0.05	5.2	0.7	3.9	0.11	
112730.71+423039.0	171.877963	42.510858	0.5310	391± 4	0.52	19050	17300	18079	3.3	-1.81	67.3	4.9	0.75	0.31	
112822.41+482309.9	172.093398	48.386109	0.5428	370± 1	0.57	4450	2850	3565	16.	-0.83	2.7	0.0	15.	0.077	
112912.27+422853.9 <sup>†</sup>	172.301146	42.481651	0.5805	308± 3	0.74	6250	4500	5362	4.6	-1.16	15.4	0.0	0.57	0.58	
113355.22+111208.8	173.480118	11.202465	0.7612	706± 4	0.65	10250	5400	7829	6.4	-1.91	4.5	0.0	0.98	0.46	
113807.83+531231.7	174.532647	53.208815	0.7899	843± 3	0.36	4700	2750	3790	1.1	-1.38	5.8	0.0	3.5	0.23	
114043.62+532439.0	175.181765	53.410835	0.5304	886± 4	0.37	3650	1350	2612	4.5	-1.69	17.9	3.3	8.4	0.039	
114915.30+393325.4 <sup>†</sup>	177.313775	39.557076	0.6284	1291± 7	0.46	5050	1600	3326	4.2	-1.25	23.9	1.2	0.33	0.90	
115816.72+132624.1 <sup>†</sup>	179.569678	13.440048	0.4389	949± 2	0.60	8650	4750	6484	7.7	-1.62	18.2	0.1	0.65	0.85	
121113.38+121937.3	182.805763	12.327049	0.4641	1441± 4	0.18	3950	600	2076	3.1	-0.78	24.4	0.0	2.1	0.11	
121303.40-014450.9	183.264183	-1.747485	0.6123	684± 3	0.37	4200	2350	3250	7.8	-1.27	11.6	0.0	1.9	0.29	
122043.21-013215.3	185.180046	-1.537600	0.4478	915± 6	0.33	2100	100	990	1.8	-1.41	160.5	6.5	12.	0.011	
124300.87+153510.6	190.753663	15.586296	0.5609	1173± 2	0.16	1700	0	856	5.5	-1.56	37.5	0.7	9.2	0.043	
125057.57+402100.3	192.739909	40.350086	0.6070	1789± 8	0.05	8350	2550	4427	3.9	-1.25	3.0	1.2	1.2	0.24	
125942.80+121312.6 <sup>†</sup>	194.928337	12.220168	0.7487	2716± 10	0.49	13400	2250	7892	12.	-0.57	14.7	0.0	0.93	0.94	
130741.12+503106.5	196.921364	50.518476	0.6987	1714± 3	0.09	6250	2500	4127	13.	-0.81	0.61	0.0	22.	0.042	
131823.73+123812.6	199.598896	12.636836	0.5848	1804± 5	0.07	4150	700	2384	3.2	-1.51	4.9	4.9	7.1	0.033	
132114.42+020225.0	200.310112	2.040294	0.5813	445± 4	0.58	5050	3200	4059	3.2	-0.56	17.6	0.0	0.95	0.24	
133936.69+111949.2	204.902879	11.330361	0.6489	382± 4	0.65	7050	5300	6199	4.9	-1.34	9.1	0.6	0.91	0.39	
134415.75+331719.1 <sup>†‡</sup>	206.065639	33.288650	0.6856	771± 2	0.30	1800	0	901	7.7	-1.28	112.4	5.2	0.82	0.68	
135418.26+585935.9	208.576089	58.993326	0.7907	827± 5	0.38	3850	1750	2893	6.3	-0.81	33.1	1.7	1.1	0.40	
140025.53-012957.0	210.106416	-1.499180	0.5839	1013± 5	0.38	20000	17400	18844	6.5	-0.98	4.0	0.0	3.3	0.14	
142649.24+032517.7	216.705181	3.421588	0.5295	480± 3	0.63	3450	1600	2637	5.3	-1.25	5.9	0.0	4.4	0.086	
142927.28+523849.5	217.363680	52.647085	0.5939	1009± 2	0.63	5900	2050	3957	15.	-1.25	8.2	0.0	2.9	0.38	
143303.27+403105.1	218.263643	40.518104	0.4452	680± 4	0.38	3350	1200	2324	2.4	-1.80	15.9	1.2	1.9	0.089	
143828.63+452108.6	219.619318	45.352395	0.4268	324± 3	0.74	8250	6500	7367	3.2	-1.95	18.8	0.3	0.67	0.34	



Table 2—Continued

Name <sup>a</sup>	R.A. J2000	Decl. J2000	Redshift	AI km s <sup>-1</sup>	$depth_{max}^b$	$V_{max}^c$ km s <sup>-1</sup>	$V_{min}^d$ km s <sup>-1</sup>	$V_{ave}^e$ km s <sup>-1</sup>	$\lambda L_{\lambda}(5100\text{\AA})$ 10 <sup>44</sup> erg s <sup>-1</sup>	$\beta_{[3K,4K]}$	$EW_{[O III]}$ Å	$EW_{[Ne V]}$ Å	$M_{BH}$ 10 <sup>8</sup> M <sub>⊙</sub>	$L/L_{EDD}$
144642.26+454631.0	221.676097	45.775287	0.7364	675 ± 4	0.58	5450	2950	4198	12.	-1.09	0.0	0.9	4.2	0.20
145724.01+452157.7 <sup>†</sup>	224.350045	45.366055	0.7175	1691 ± 5	0.62	14200	6800	10259	8.6	-1.45	2.8	0.0	0.95	0.65
145736.70+523454.6	224.402944	52.581834	0.6376	1194 ± 4	0.68	9150	3600	6041	11.	-1.74	8.7	0.2	2.4	0.34
145836.73+433015.5	224.653068	43.504323	0.7595	615 ± 5	0.62	6500	3850	5122	9.7	-1.58	4.7	0.5	6.5	0.11
150847.41+340437.7	227.197577	34.077147	0.7880	722 ± 1	0.52	2850	200	1573	34.	-1.48	134.1	5.8	30.	0.083
152350.42+391405.2	230.960111	39.234787	0.6612	3227 ± 2	0.43	20000	11500	16458	38.	-1.14	4.8	0.1	39.	0.069
153036.82+370439.1	232.653452	37.077543	0.4170	1911 ± 5	0.44	8100	2000	4657	7.0	-1.20	13.5	0.3	1.2	0.44
160329.72+502722.2	240.873867	50.456176	0.6389	762 ± 5	0.49	5300	2800	4133	4.5	-1.61	23.3	2.3	2.4	0.13
160628.06+290333.8	241.616939	29.059398	0.4347	489 ± 3	0.63	3650	1500	2696	9.1	-0.14	8.3	4.3	1.3	0.49
160721.27+515510.6	241.838665	51.919619	0.7739	404 ± 3	0.63	6800	5200	5909	6.9	-2.19	4.7	2.3	0.88	0.57
163255.46+420407.7	248.231106	42.068816	0.7263	1152 ± 4	0.56	8650	750	3985	7.8	-1.53	18.2	4.7	39	0.014
163513.51+213859.6 <sup>†</sup>	248.806315	21.649900	0.6835	573 ± 5	0.69	6950	4300	5620	4.9	-1.57	6.3	0.3	0.61	0.58
165225.39+215830.7	253.105807	21.975220	0.4468	1155 ± 12	0.42	7850	4450	6170	3.6	-0.26	18.8	0.0	0.68	0.38
170010.83+395545.8 <sup>†</sup>	255.045127	39.929392	0.5766	462 ± 6	0.67	5550	3750	4594	3.7	-0.69	12.5	1.2	0.51	0.52
170341.82+383944.7	255.924255	38.662439	0.5539	785 ± 7	0.43	5000	2750	3949	5.9	0.01	8.1	1.9	5.0	0.084
204333.20-001104.2	310.888342	-0.184524	0.5449	2074 ± 4	0.16	8250	2750	5061	8.9	-1.12	7.7	0.0	2.0	0.31
210757.67-062010.6	316.990293	-6.336294	0.6456	2344 ± 1	0.21	8250	0	3709	27.	0.01	18.5	1.9	76.	0.026
224028.14-003813.1	340.117275	-0.636989	0.6591	1364 ± 2	0.23	3650	750	1994	9.9	-1.19	8.2	0.0	8.1	0.087

<sup>a</sup>SDSS DR5 designation, hhmmss.ss+ddmmss.s (J2000.0)<sup>b</sup>Deepest part of any BAL trough<sup>c</sup>Maximum velocity of the BAL troughs from the emission line<sup>d</sup>Minimum velocity of the BAL troughs from the emission line<sup>e</sup>Weighted average velocity of the BAL troughs<sup>†</sup>narrow-line Seyfert 1<sup>‡</sup>double-peaked narrow lines

Table 3. Parameters of Emission Lines from Composite Spectra

	N-B-H <sup>a</sup>	N-B-L	M-F-H	N-F-H	M-F-L	N-F-L	N-R-H	M-R-L	N-R-L	no[Ne V] <sup>b</sup>	[Ne V] <sup>c</sup>	nonBAL	LowV <sup>d</sup>	BAL <sup>e</sup>
$EW_{[O III]} (\text{\AA})$	38.0	12.4	58.0	36.8	8.7	10.7	38.4	5.8	10.7	8.1	19.5	18.4	21.9	14.2
[O III]	1	1	1	1	1	1	1	1	1	1	1	1	1	1
$H\beta^N$	0.051	0.035	0.060	0.068	0.098	0.16	0.071	0.11	0.098	0.26	0.19	0.084	0.058	0.19
$H\gamma^N$	0.030	0.035	0.041	0.039	0.083	0.079	0.032	0.046	0.036	0.11	0.12	0.048	0.0792	0.097
OptFeII <sup>N</sup>	0.16	0.24	0.088	0.057	3.4	1.8	0.13	1.7	0.67	4.8	0.52	0.41	0.45	2.0
[Ne V]	0.065	0.091	0.070	0.077	0.017	0.089	0.081	0.0092	0.14	0.00070	0.089	0.083	0.084	0.051
[O II]	0.070	0.051	0.083	0.097	0.14	0.11	0.15	0.29	0.18	0.083	0.078	0.14	0.11	0.15
[Ne III]	0.086	0.12	0.067	0.099	0.098	0.16	0.12	0.29	0.21	0.18	0.11	0.15	0.15	0.10
$EW_{H\beta B} (\text{\AA})$	117.7	75.7	89.9	74.9	68.4	61.1	60.3	57.5	50.6	66.5	78.4	76.9	71.6	69.5
$H\beta^B$	1	1	1	1	1	1	1	1	1	1	1	1	1	1
$H\gamma^B$	0.28	0.23	0.24	0.24	0.25	0.24	0.26	0.29	0.21	0.26	0.21	0.25	0.23	0.24
OptFeII <sup>B</sup>	0.77	2.2	0.79	1.4	3.5	3.6	1.4	3.3	3.2	3.7	2.4	2.2	2.2	2.7

<sup>a</sup>Names of the composite spectra: X-Y-Z

X: N- non-Mg II BAL quasar; M- Mg II BAL quasar

Y: B-  $\beta_{[3K,4K]} \leq -2.2$ ; F-  $-2.2 < \beta_{[3K,4K]} \leq -1$ ; R-  $\beta_{[3K,4K]} > -1$

Z: H-  $EW_{[O III]} \geq 20 \text{\AA}$ ; L-  $EW_{[O III]} < 20 \text{\AA}$

<sup>b</sup>The composite spectrum of non-Mg II BAL quasars with  $S/N > 20$  and undetectable [Ne V] emission

<sup>c</sup>The composite spectrum of non-Mg II BAL quasars with  $S/N > 20$  and detectable [Ne V] emission

<sup>d</sup>The composite spectrum of  $1000 \text{ km s}^{-1} \leq \Delta v_c < 1600 \text{ km s}^{-1}$  selected quasars in low- $z$  quasar sub-sample

<sup>e</sup>The composite spectrum of  $\Delta v_c \geq 1600 \text{ km s}^{-1}$  selected Mg II BAL quasars in low- $z$  quasar sub-sample

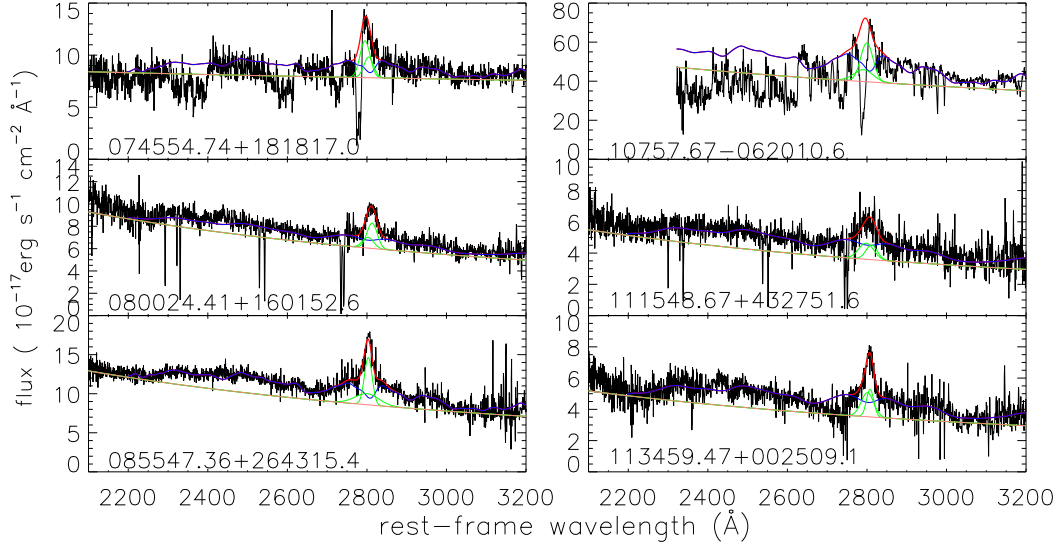


Fig. 1.— Observed spectra overlaid with the best-fit models for the six quasars in the high- $z$  sample. The models are described in detail in §2.1. In each panel, we plot the observed spectrum in black curves, power-law continuum in pink, broadened Fe II template in blue, Gaussian Mg II emission line in green, and the model sum in red.

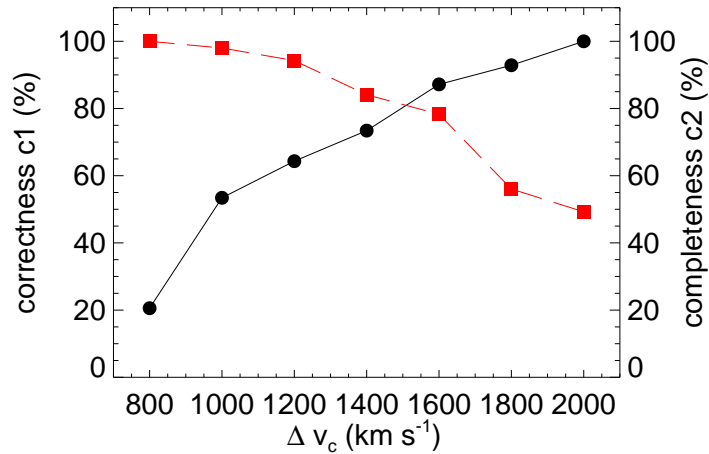


Fig. 2.— Correctness  $c1$  (black filled circles) and completeness  $c2$  (red filled squares) of BAL quasars as a function of Mg II absorption-line width cutoff  $\Delta v_c$ .

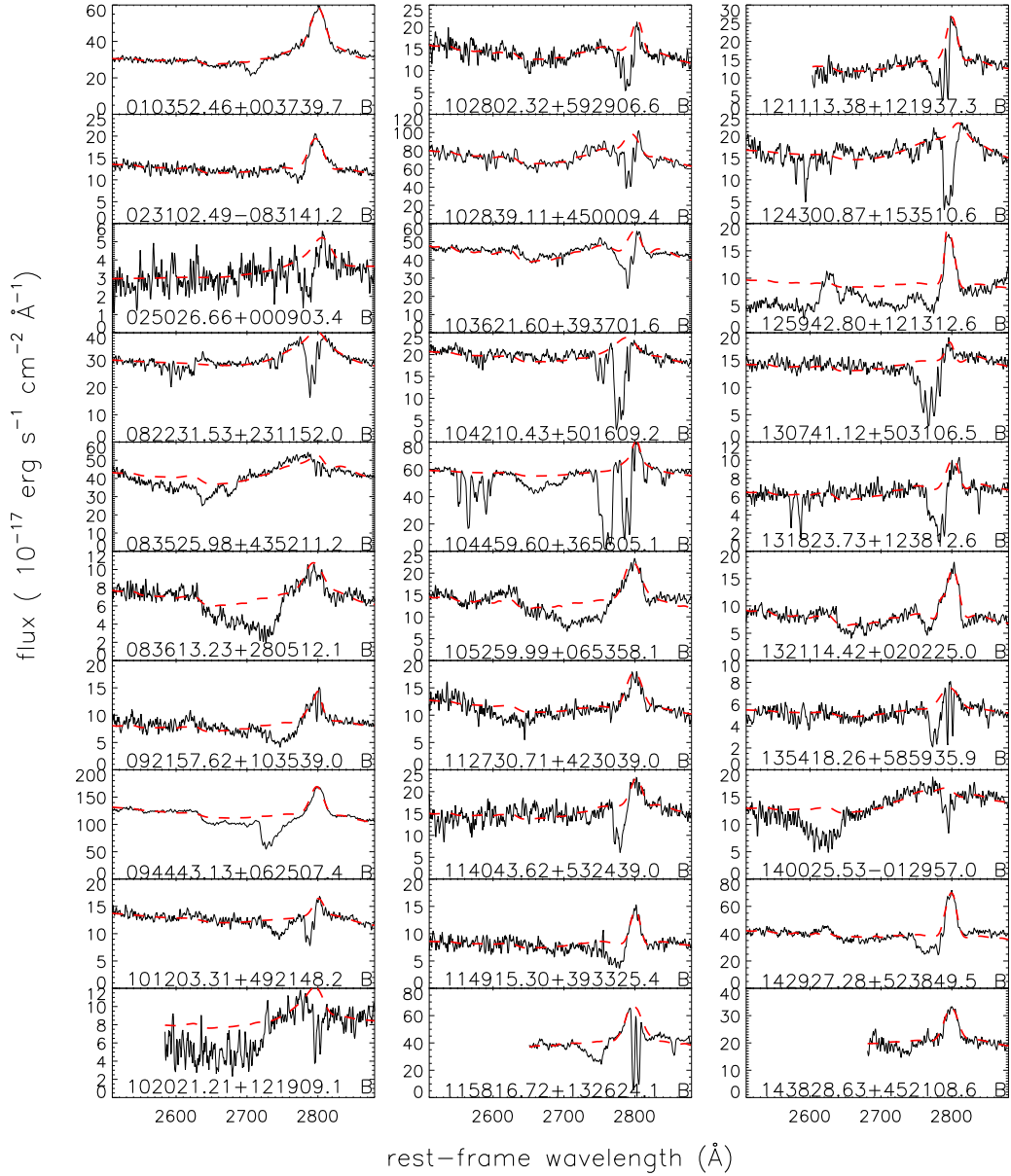


Fig. 3.— Observed spectra and our best-fit models of the low- $z$  sample of 68 Mg II BAL quasars, including 41 classified as such by both of us and G09 (marked with "B"), and 27 in this work but not in G09 (marked with "A"). Also shown here are eight objects that are not classified as Mg II BAL quasars according to our new criterion, but are classified as such in G09 (marked with "L").

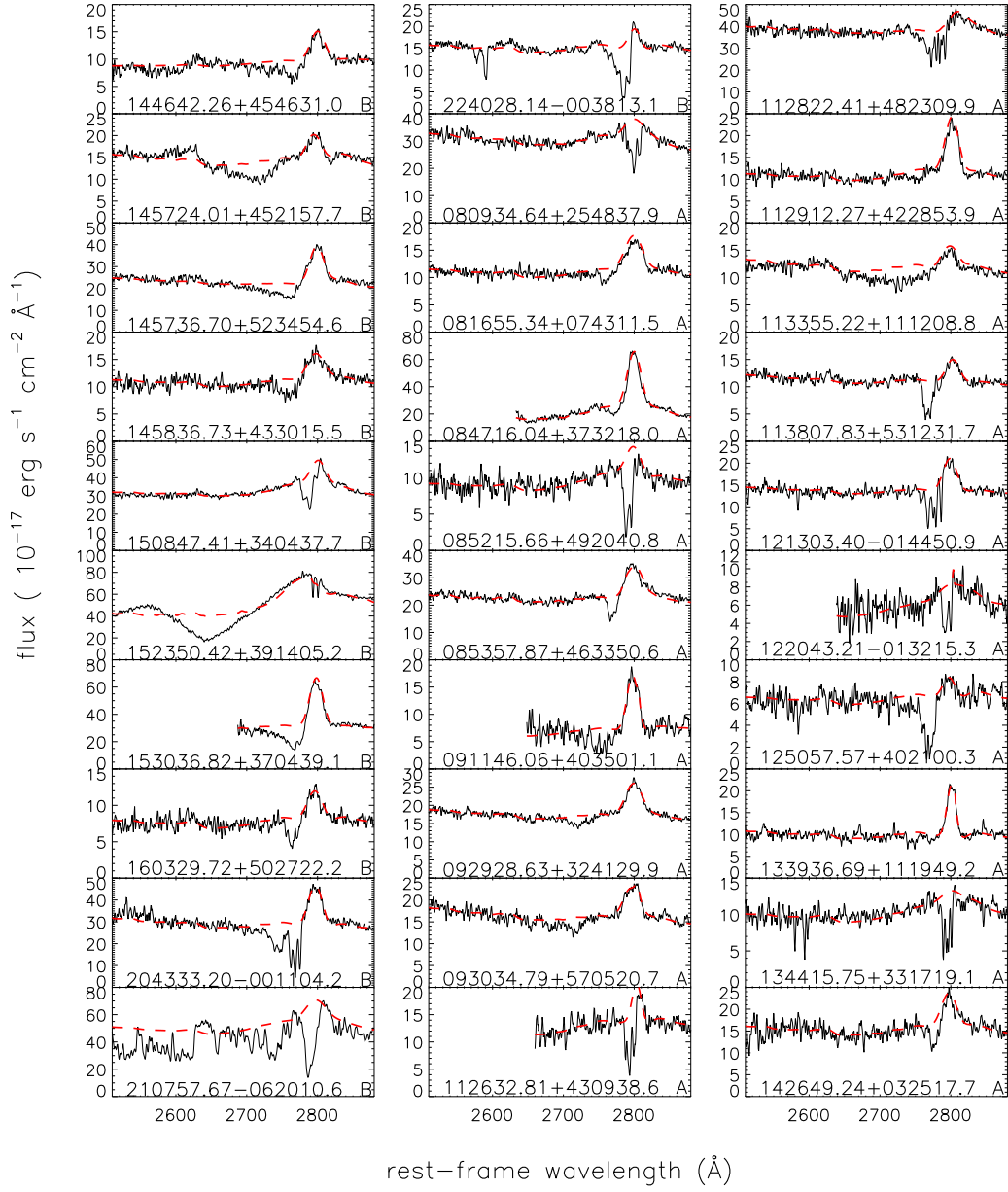


Fig. 3.— Continued...

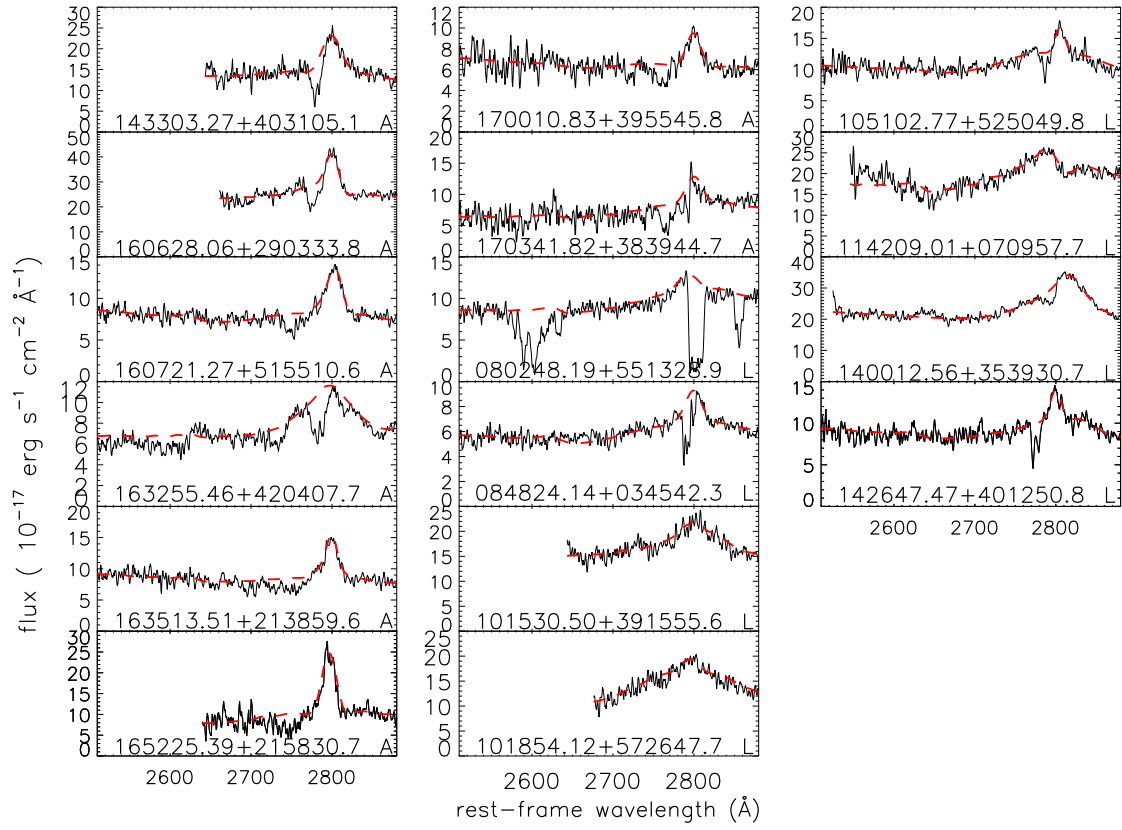


Fig. 3.— Continued.

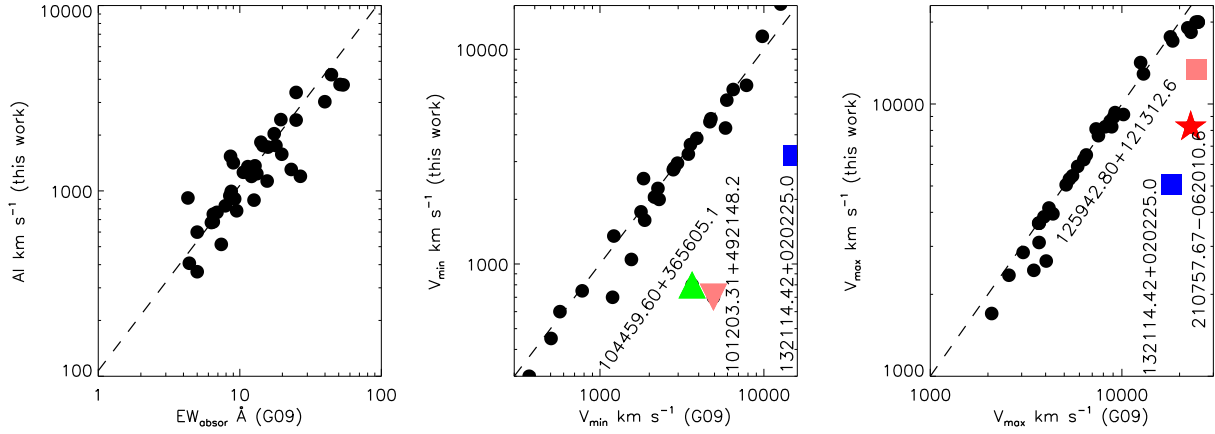


Fig. 4.— Comparison of Mg II BAL parameters between our measurements and G09’s. The 41 objects in the low- $z$  sample are classified as Mg II BAL quasars in this work and G09. *Left:* absorption index ‘AI’ vs. rest-frame equivalent width, *middle:* minimum velocity  $V_{min}$ , and *right:* maximum velocity  $V_{max}$ . The dashed lines show one-to-one correspondence. Overall, our measurements agree well with that of G09. Significant differences are found for five quasars. The origin of the discrepancies examined in §2.3 and the observed spectra of these five quasars are shown in Fig. 3, together with our best-fit models.

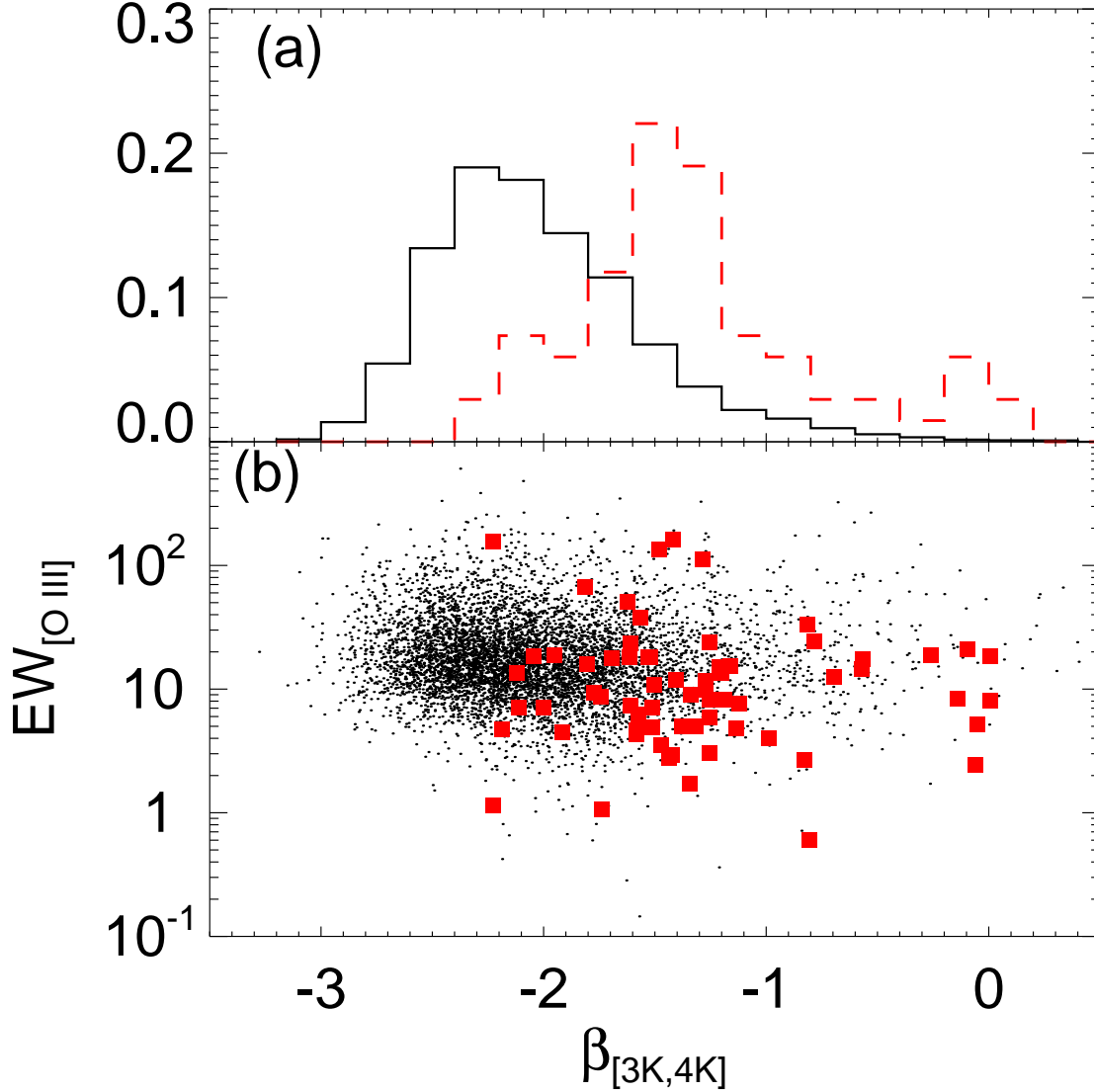


Fig. 5.— Panel (a): Comparison of the distribution of continuum slope  $\beta_{[3K,4K]}$  between Mg II BAL quasars (red dash line) and non-loBAL quasars (black thick line). It is obvious that Mg II BAL quasars are much redder than non-loBAL quasars. The  $\beta_{[3K,4K]}$  distribution of non-Mg II BAL quasars peaks at -2.2, much less than the value of -1.7 for Mg II BAL quasars. The median value of  $\beta_{[3K,4K]}$  is -2.08 for non-Mg II BAL quasars, and it is -1.41 for Mg II BAL quasars. Panel (b): Equivalent width of O III NEL  $EW_{[O III]}$  plotted against continuum slope  $\beta_{[3K,4K]}$  for the low- $z$  sample. Mg II loBAL quasars are shown in filled red squares, and non-loBAL quasars in filled black circles.



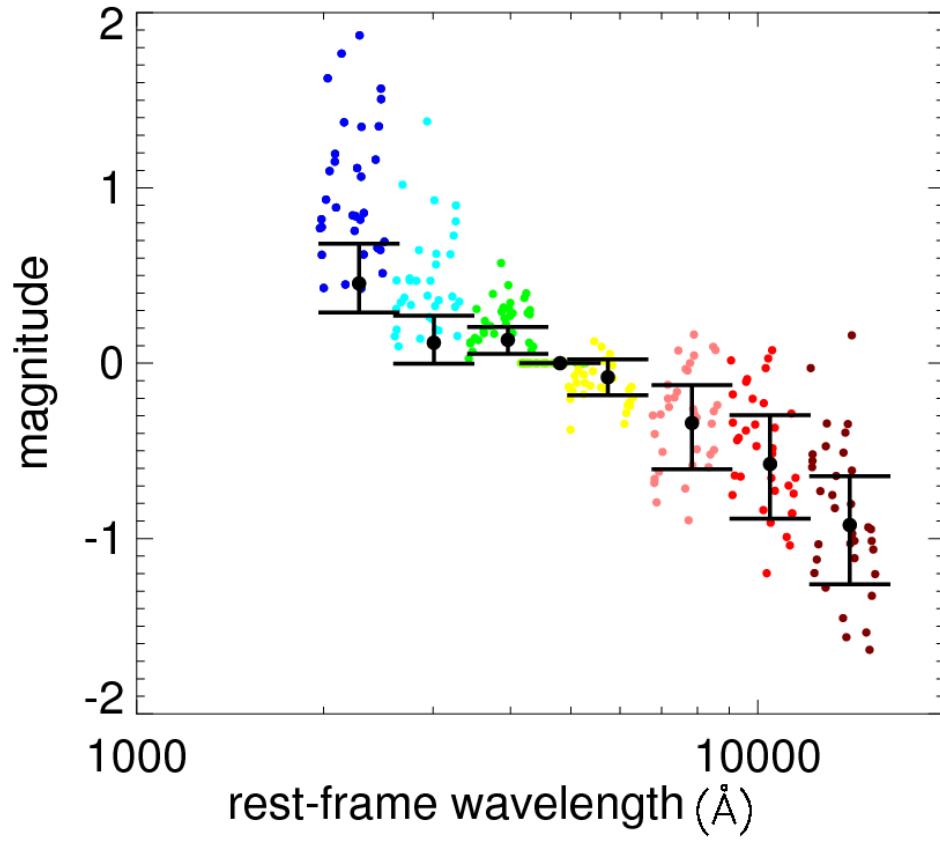


Fig. 6.— Comparison of the UV-optical-NIR SED of Mg II BAL and non-loBAL quasars. All the data are normalized at the SDSS  $i$ -band. The different bands of Mg II BAL quasars are shown by filled circle in different colors. The black filled circles show the mean SED of non-loBAL quasars, with the upper and lower quartile denoted by error bars.

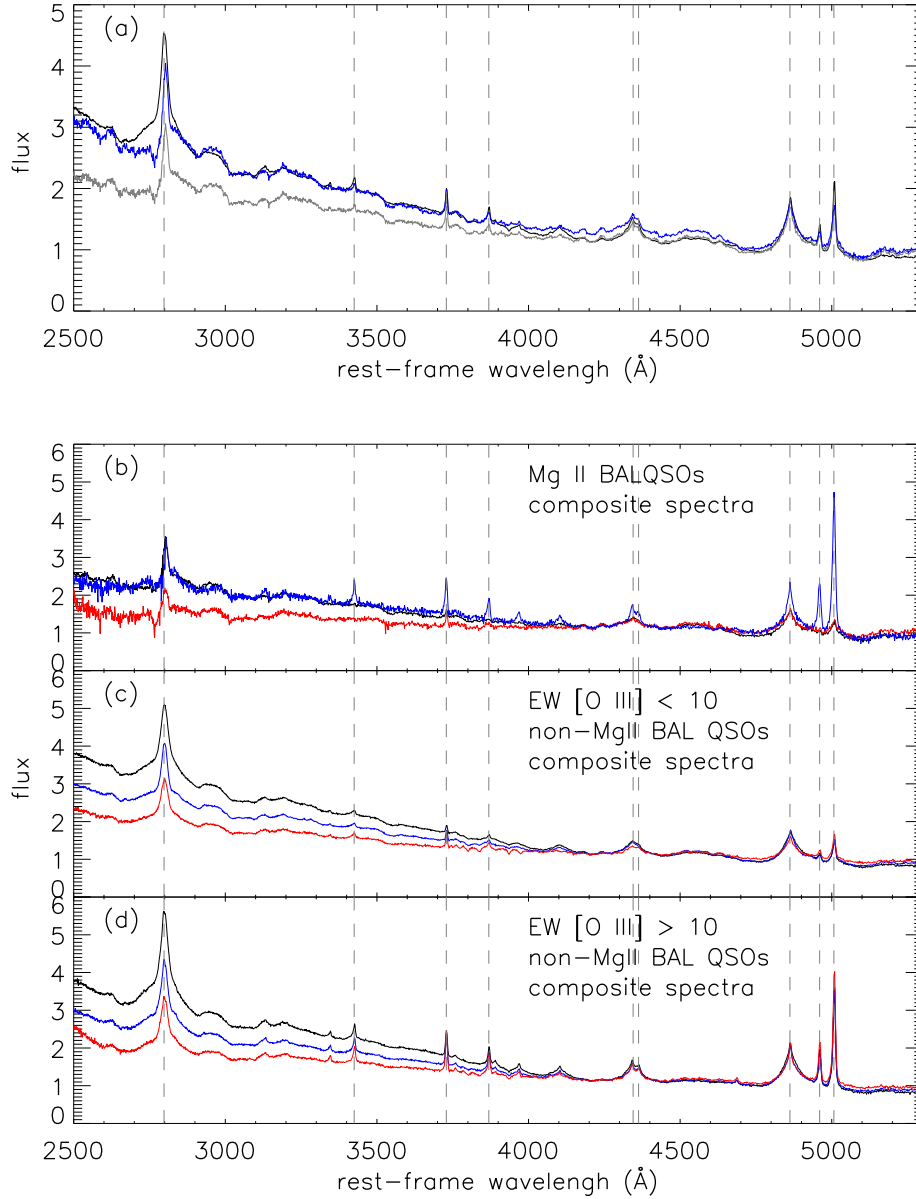


Fig. 7.— Panel (a)—Composite spectra of the full non-Mg II BAL quasars sample(black), Mg II BAL quasars sample(gray) and the blue curve is the de-reddened composite spectra of Mg II BAL quasars; Panel (b)—Composite spectra of the Mg II BAL quasars with different continuum color and intensity of [O III] emission line, black for the flat and [O III]-weak sources, red means red and [O III]-weak and blue curve shows the Mg II BAL composite with flat and [O III]-strong; Panel (c) and (d)—Composite spectra of the quasars without Mg II broad absorption troughs. The three colors (black, blue and red) means that continuum slopes are blue, flat and red. (see the text §3.2)

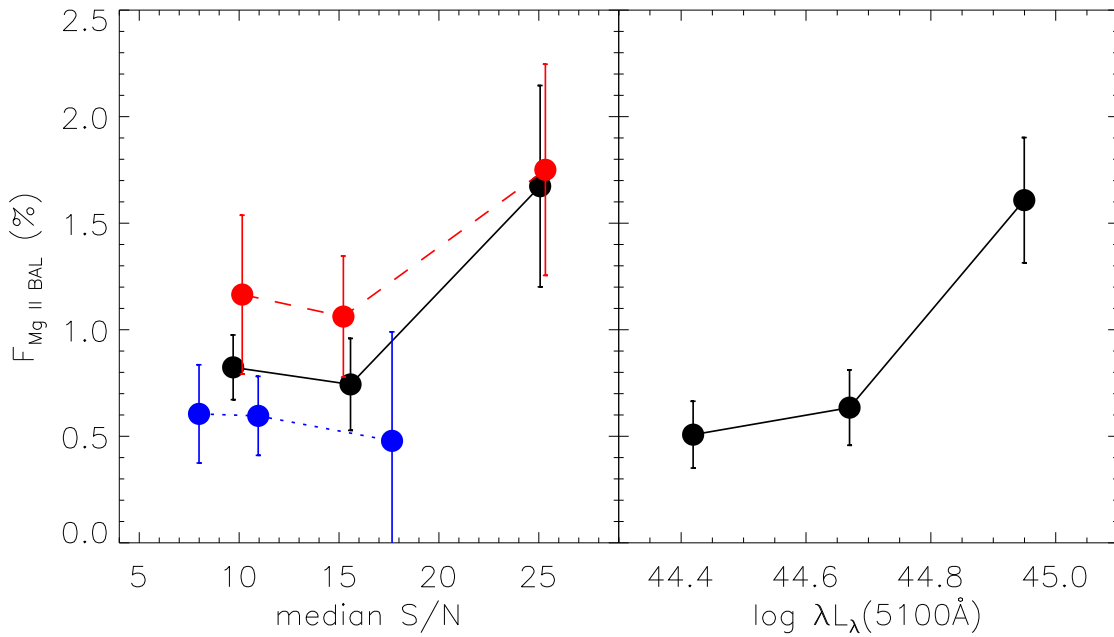


Fig. 8.— Fraction of Mg II BAL quasars in the low- $z$  sample as a function of the median  $S/N$  ratio of the SDSS spectra (left panel) and the luminosity at 5100Å(right panel). The median  $S/N$  ratios are calculated in the rest-frame wavelength range of 2820 – 3200 Å. The whole sample are shown in black, and the high and low luminosity sub-samples are shown in red and blue, respectively. The two luminosity sub-samples are so carved that they have the same number of quasars.

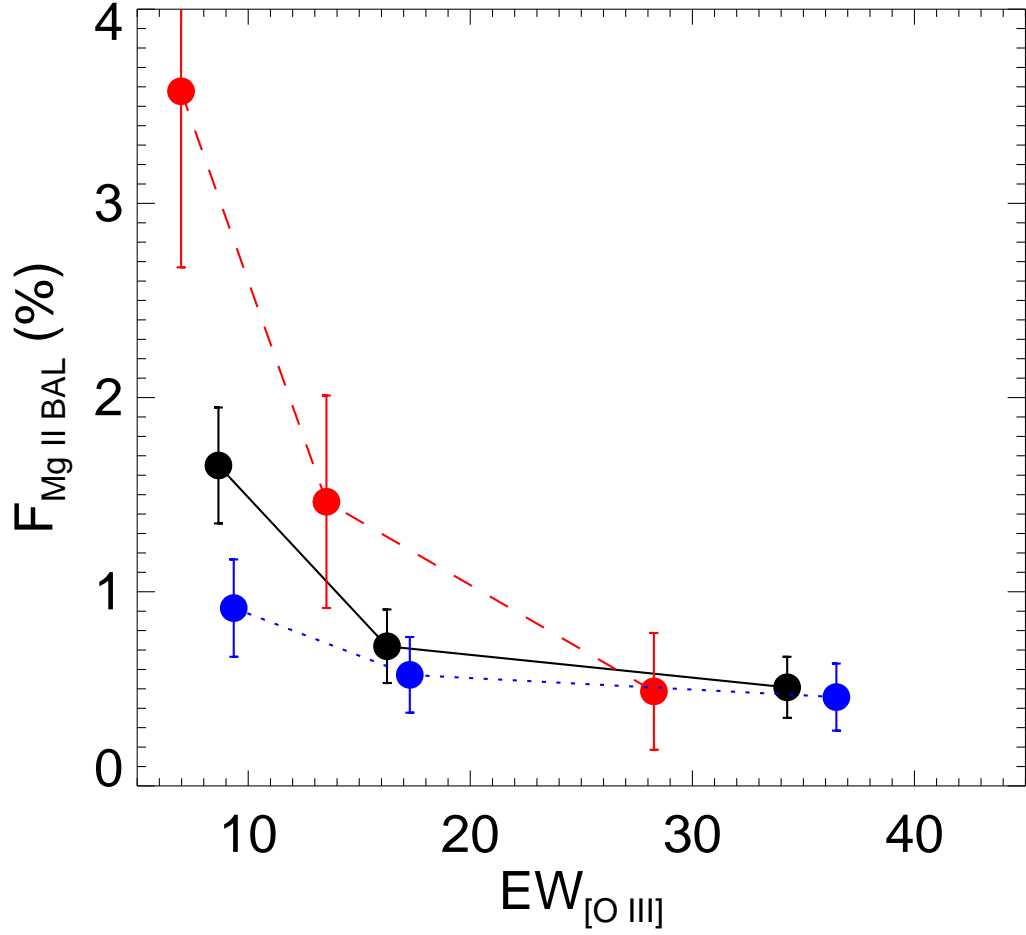


Fig. 9.— Fraction of Mg II BAL quasars observed in low- $z$  sample as a function of the equivalent width of [O III]  $\lambda 5007$  NEL (black). Each point in the plot represents the fraction of Mg II BAL quasars in a bin of 2522 quasars arranged in order of increasing  $EW_{[O III]}$ . The x-coordinate of each point represents the median value of the bin. The "error bars" represent  $1\sigma$  limits on the fractions calculated using a binomial distribution. We also show the connection in the two  $\lambda L_{\lambda}(5100\text{\AA})$  quasar bins, the red and blue lines correspond to the high and low  $\lambda L_{\lambda}(5100\text{\AA})$  bins.

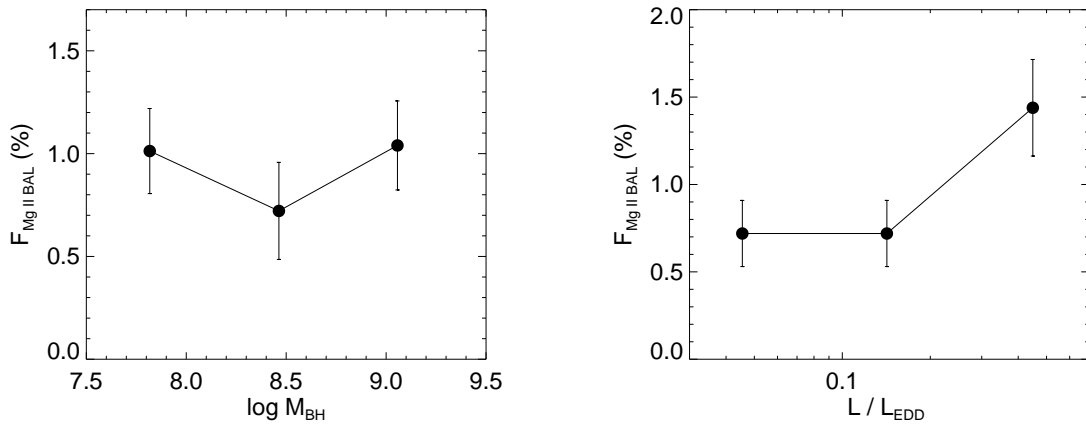


Fig. 10.— Fraction of Mg II BAL quasars in the low- $z$  sample as a function of black hole mass (left panel) and Eddington ratio (right panel).

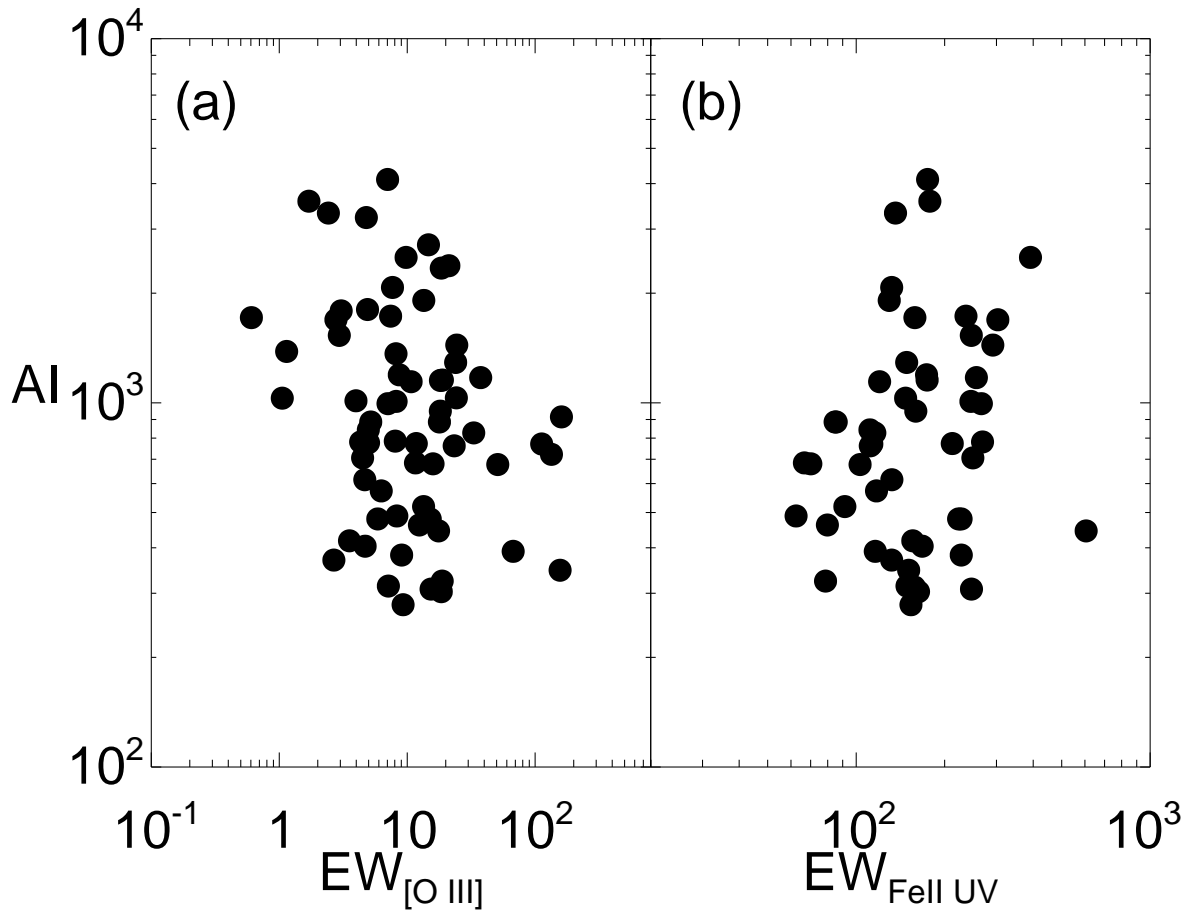


Fig. 11.— Plots of Mg II absorption index against the equivalent width of [O III] (left panel) and UV Fe II (right panel) emission lines.

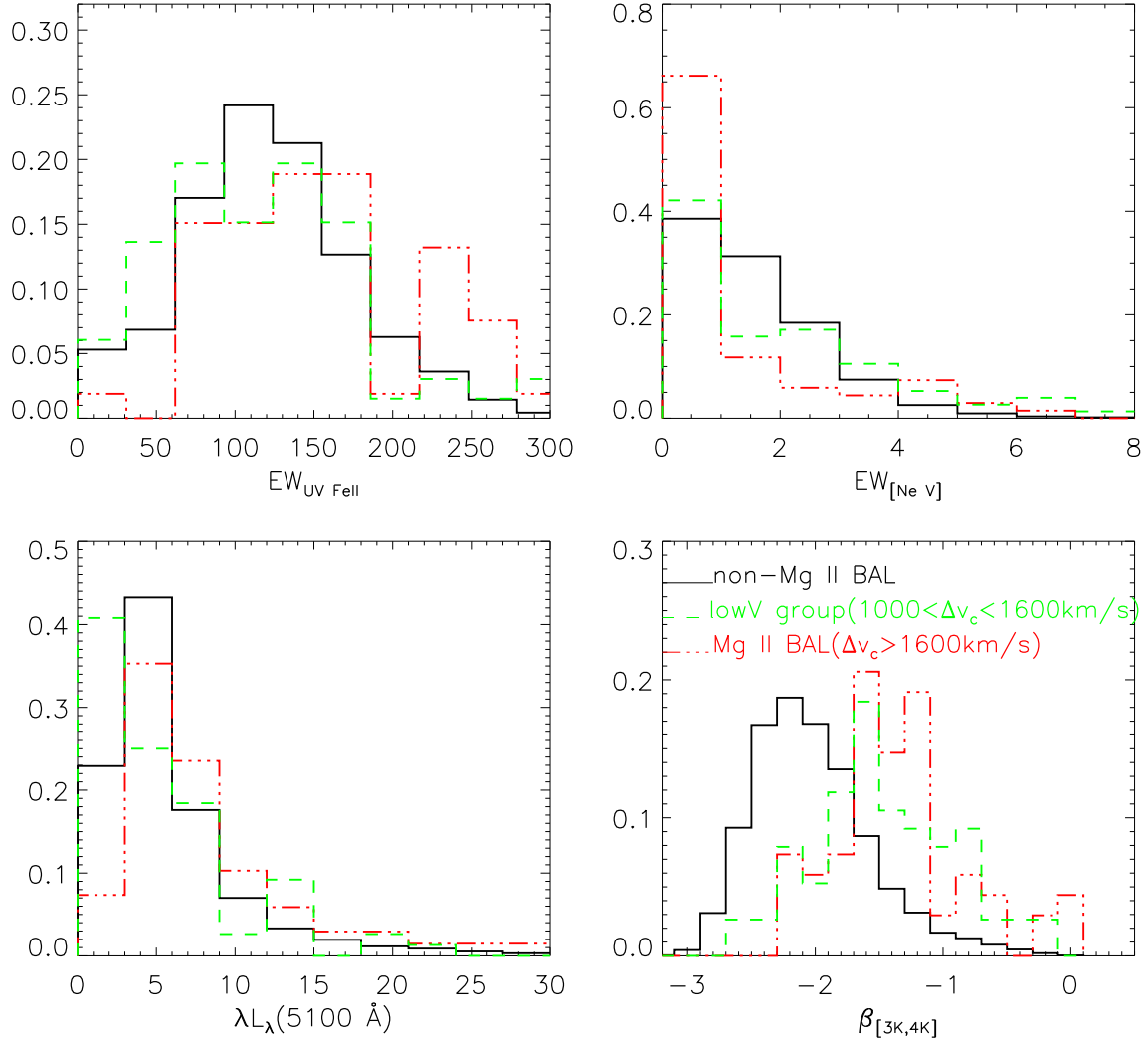


Fig. 12.— Statistical properties of lowV group (green) and Mg II BAL quasar sample (red). The black line are non-loBAL quasars as the comparison sample.

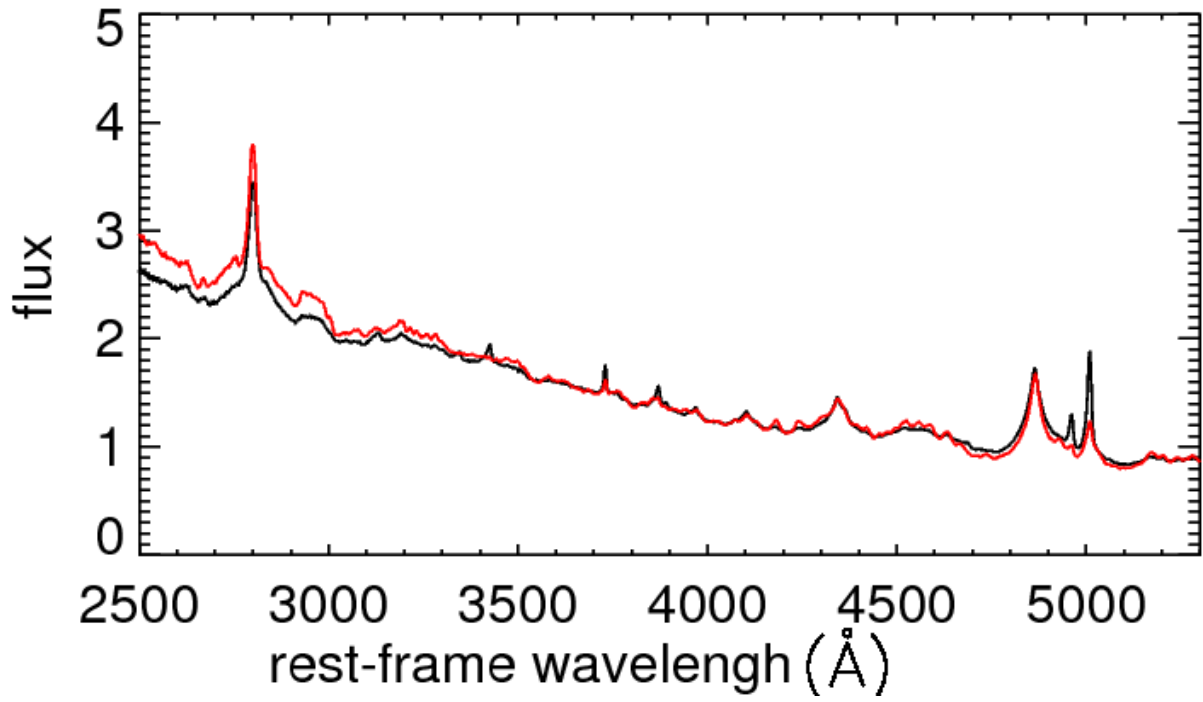


Fig. 13.— Composite spectrum of non-loBAL quasars with/without detectable [Ne V] emission.